



Hydrological Cycle Intensification and Permafrost Thaw Drive Increased Freshwater and Organic Carbon Inputs to Northern Alaska Estuaries

Item Type	Article
Authors	Rawlins, Michael;Connolly, Craig;McClelland, James W
Citation	Rawlins, M. A., Connolly, C. T., & McClelland, J. W. (2026). Hydrological cycle intensification and permafrost thaw drive increased freshwater and organic carbon inputs to northern Alaska estuaries. <i>Global Biogeochemical Cycles</i> , 40, e2025GB008822. https://doi.org/10.1029/2025GB008822
DOI	10.1029/2025GB008822
Rights	Attribution 4.0 International
Download date	2026-06-11 07:48:54
Item License	http://creativecommons.org/licenses/by/4.0/
Link to Item	https://hdl.handle.net/20.500.14394/58379

Global Biogeochemical Cycles®






RESEARCH ARTICLE

10.1029/2025GB008822

Special Collection:

Changing biogeochemical cycles along the land-to-ocean aquatic continuum

Hydrological Cycle Intensification and Permafrost Thaw Drive Increased Freshwater and Organic Carbon Inputs to Northern Alaska Estuaries

Michael A. Rawlins¹ , Craig T. Connolly² , and James W. McClelland³ 

¹Department of Earth, Geographic, and Climate Sciences, University of Massachusetts, Amherst, MA, USA, ²Marine Sciences Institute, University of Texas at Austin, Port Aransas, TX, USA, ³The Ecosystems Center, Marine Biological Laboratory, Woods Hole, MA, USA

Key Points:

- Fluxes were quantified for the entire Alaska North Slope and specific watersheds and receiving estuaries to assess patterns in land-sea coupling
- Inputs to individual lagoons, bays, and sounds reflect influences from landscape composition and contributing basin size
- Effects of hydrological cycle intensification and permafrost thaw are evident in temporal trends, with implications for coastal ecosystems

Supporting Information:

Supporting Information may be found in the online version of this article.

Correspondence to:

M. A. Rawlins,
mrawlins@umass.edu

Citation:

Rawlins, M. A., Connolly, C. T., & McClelland, J. W. (2026). Hydrological cycle intensification and permafrost thaw drive increased freshwater and organic carbon inputs to northern Alaska estuaries. *Global Biogeochemical Cycles*, 40, e2025GB008822. <https://doi.org/10.1029/2025GB008822>

Received 8 AUG 2025

Accepted 24 FEB 2026

Author Contributions:

Conceptualization: Michael A. Rawlins

Data curation: Craig T. Connolly, James W. McClelland

Formal analysis: Michael A. Rawlins

Funding acquisition: Michael

A. Rawlins, James W. McClelland

Investigation: Michael A. Rawlins, Craig T. Connolly, James W. McClelland

Methodology: Michael A. Rawlins

© 2026. The Author(s).

This is an open access article under the terms of the [Creative Commons Attribution License](https://creativecommons.org/licenses/by/4.0/), which permits use,

distribution and reproduction in any medium, provided the original work is properly cited.

Abstract Understanding how hydrological inflows and climate change influence individual estuaries across northern Alaska is limited by a paucity of measured data, necessitating the application of suitably scaled numerical process models. This study uses an updated model to quantify freshwater discharge and dissolved organic carbon (DOC) export from the North Slope of Alaska (NSA) to coastal waters of the Beaufort Sea and examines climate-linked temporal changes. The model was applied at 1 km resolution across the 166,483 km² NSA domain over 1980–2023. Watershed inputs to coastal waters were estimated by routing along river networks to 1,039 outlets at the land-sea boundary. Key simulation parameters were evaluated to demonstrate model efficacy, then spatial and temporal patterns were quantified. Exports to specific lagoons, bays, and sounds demonstrate how landscape composition, terrestrial drainage basin size, and estuary area modulate watershed influence on coastal ecosystems across the region. Freshwater discharge and DOC export increased over the greater than four decades, associated with changes in precipitation and permafrost thaw. Surface and supra-permafrost subsurface fluxes also increased, with pronounced rises in proportional contributions via subsurface flow during summer and autumn. These changes have the potential to substantially impact salinity and trophic conditions along Alaska's Beaufort Sea coast. Our study highlights the value of model-data syntheses that resolve regional-to-local scale fluxes where observational measurements are sparse, and provides novel quantitative export metrics that will be useful to researchers, resource managers, and other stakeholders with interests in the climate, hydrology, and biogeochemistry of coastal northern Alaska.

Plain Language Summary Watershed inputs from land drive coastal ecosystem dynamics in the Arctic, yet understanding of how they vary over space and time is limited by a scarcity of measured and modeled data. This study applies an updated numerical model that provides estimates of freshwater discharge and dissolved organic carbon (DOC) export from land to individual estuaries along the Alaskan Beaufort Sea coast. The model was developed for the North Slope of Alaska, with sufficient resolution and scaling to estimate watershed inputs to individual lagoons, bays, and sounds between Point Barrow and the US-Canada border. Model results, covering 1980–2023, show (a) that landscape characteristics drive spatial variability in freshwater and DOC export to individual estuaries, and (b) a significant increase in freshwater and DOC inputs to the Alaskan Beaufort Sea over time. These changes manifest in surface and subsurface (groundwater) flow, but the proportion of subsurface flow also increased. An enhanced water cycle is increasing flows, while deeper soil thaw in summer is causing more DOC to reach the coast. The changes demonstrated in this study are likely altering salinity, biogeochemical processes, and food web relationships in the coastal Beaufort Sea.

1. Introduction

Rivers are defining features of the land-ocean system, playing crucial roles as conduits for the transport of water and water-borne materials from terrestrial landscapes to the marine environment. Their impact on ocean processes is particularly strong in the Arctic, where 11% of the world's river water is delivered to an ocean basin that contains about 1% of the world's ocean volume (Aagaard & Carmack, 1989; McClelland et al., 2012). Notably, Arctic rivers deliver ~34 Tg C of dissolved organic carbon (DOC) and 8 Tg C of particulate organic carbon (POC) per year to the Arctic Ocean and surrounding seas (Fabre et al., 2024). Respiration of this river-supplied organic matter is a significant component of the global carbon (C) cycle, amounting to annual atmospheric emissions of 250 Tg C (Liu et al., 2022). Arctic river DOC and POC export also drive local ecosystem processes, serving as

Visualization: Michael A. Rawlins, Craig T. Connolly

Writing – original draft: Michael A. Rawlins

Writing – review & editing: Michael A. Rawlins, Craig T. Connolly, James W. McClelland

important sources of energy for microbial and metazoan food webs (Connelly et al., 2015; Harris et al., 2018; Kellogg et al., 2019). Climate warming is having pervasive effects on high-latitude freshwater and organic matter export primarily due to hydrological cycle intensification and permafrost thaw (Carmack et al., 2016; Koch & O'Donnell, 2025; Rawlins & Karmalkar, 2024; Tank et al., 2023). Permafrost thaw can be expected to cause proportionally more water rerouting through subsurface pathways before entering stream networks (Bense et al., 2009; Walvoord & Kurylyk, 2016; Wang et al., 2021), potentially causing additional impacts to aquatic ecosystems. Changes to the Arctic hydrologic cycle and to the heterogeneous landscapes that Arctic rivers drain will both alter lateral (land-ocean) and vertical (land-atmosphere) carbon fluxes as climate warming continues (Vonk et al., 2025).

A few large rivers that have been extensively studied over the past 20 years export a majority of freshwater and land-derived materials from the pan-Arctic drainage basin to the Arctic Ocean (Holmes et al., 2011; McClelland et al., 2016; Tank et al., 2023). There is, however, increasing recognition that inputs from smaller watersheds are also regionally important. These watersheds are located relatively close to the land-sea interface (Speetjens et al., 2023) and often manifest much higher DOC yields because they drain low-gradient terrain and are underlain by continuous permafrost that constrains water movement to shallow, organic-rich soils in the seasonal active layer (McClelland et al., 2014; Starr et al., 2023). Beyond their outsized role in DOC transport, small watersheds that abut the coast may be experiencing different climate change effects such as enhanced warming rates (Vonk et al., 2023), and greater precipitation and runoff amounts during this century (Rawlins & Karmalkar, 2024).

On the North Slope of Alaska, small-to-medium sized rivers drain into a diverse array of lagoons, bays, and sounds along the Beaufort Sea coast between Point Barrow to the west and the Alaska-Canada border to the east. Studies focusing on the Colville, Kuparuk, and Sagavanirktok rivers have fostered foundational understanding of seasonal fluvial export from the North Slope to the Beaufort Sea (McClelland et al., 2014), while numerous studies of inland streams and rivers have explored relationships between basin characteristics and associated fluxes at smaller catchment scales (e.g., Khosh et al., 2017; Shogren et al., 2020, 2024). Our understanding of seasonal and long-term export from small drainage areas near the coast, on the other hand, is less well developed.

The paucity of field data from these catchments presents a barrier to advancing understanding of Arctic land-ocean biogeochemical coupling. Numerical models have become increasingly valuable to help fill this void, but these models are often difficult to develop across spatially and temporally variable regional systems. Numerical models also have the added benefit of generating long-term estimates that can integrate the myriad of change resulting from climate warming. This is particularly true in the Arctic where the scientific basis for model parameterization is still growing (Bertin et al., 2023; Clark et al., 2022; Gibson et al., 2022). To meet these challenges, hydrological and biogeochemical models designed for high-latitude systems need to be suitably scaled and parsimonious enough to simulate key processes and the complex interactions between seasonality, water availability, soil freeze-thaw, and carbon mobilization (Kicklighter et al., 2013; Mohammed et al., 2022; Rawlins et al., 2013, 2021). While these models are being developed for large Arctic rivers, which can leverage broader (but coarser) spatial data sets (Clark & Mannino, 2021; Song et al., 2025), finer spatial resolution models with requisite input data are needed to accurately quantify water and DOC export for the many smaller rivers that influence nearshore coastal environments (Spera et al., 2026). Developing and implementing effective and efficient physically based process models is all the more challenging. In a recent effort, Rawlins et al. (2021) described a process model applied at 25 km resolution that was capable of estimating export from individual medium and large northern Alaska rivers. In a subsequent study, the same model was downscaled to 1 km resolution for the coastal catchment draining into Elson Lagoon (Rawlins, 2021), demonstrating that a finer resolution model was needed to investigate terrestrial exports to individual coastal features. We expand on that effort to refine and employ a process model that accurately quantifies exports across the wide range of stream and river sizes that drain the entire North Slope of Alaska.

In this study we apply and analyze simulation estimates over 1980–2023 to quantify river discharge and DOC exports and their temporal trends across the North Slope of Alaska to the Beaufort Sea coast. Using these estimates, we further investigate connections to individual lagoons, bays, and sounds to understand how these exports and their influence vary across individual coastal features. First, elements of the study spatial domain and river network are introduced, followed by descriptions of the model process representations, parameterizations and meteorological forcings. We then discuss model evaluations of key simulation elements supporting model efficacy in characterizing and quantifying riverine exports. Next, results focused on discharge and DOC spatial and

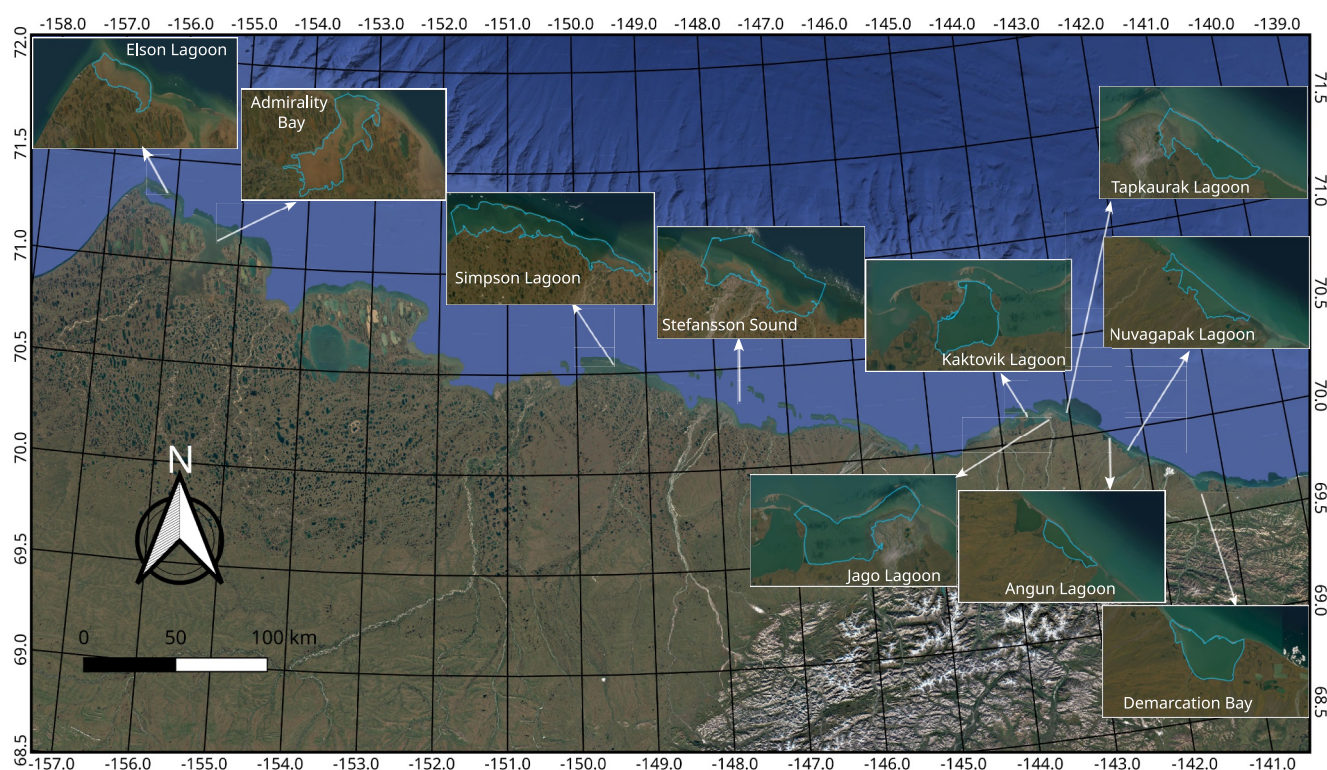


Figure 1. Lagoons, bays, and sounds along the Northern Alaska coast into which freshwater flux and DOC exports are estimated. The study domain includes all land areas draining to the coast from the Clarence River at the easternmost edge of the domain near Demarcation Bay westward to Point Barrow near Utqiagvik, Alaska.

temporal patterns are described. Lastly, a trend analysis is presented to evaluate how aspects of climate change have affected exports and may be influencing coastal ecosystems.

2. Model Specifications and Forcings

2.1. Spatial Domain and River Network Specifications

The study area (166,483 km²) encompasses all land draining the North Slope of Alaska (NSA) to the Beaufort Sea. Spatial resolution for the model simulation is 1 × 1 km on the Northern Hemisphere Equal Area Scalable Grid (EASE-Grid) v2 (Brodzik et al., 2012). The NSA is bounded in the south by the Brooks Range, which approaches the coast in the eastern part of the region. This physiographic pattern causes rivers to drain proportionally more mountainous terrain in the eastern region of the NSA compared to the west (Connolly et al., 2018). The most actively studied major rivers draining the NSA are the Colville (basin area 59,647 km²), Sagavanirktok (13,465 km²), and Kuparuk (9,101 km²). While these three rivers drain nearly half (49.4%) of the NSA, their fluxes funnel into a concentrated area that makes up only 13% of the Alaska Beaufort Sea coastline. To define river basin drainage areas and route water and DOC to the coast, we use a digital river network derived from ArcticDEM 100 m elevation data mapped on the same 1 km² EASE-Grid domain. Exports are calculated for all land areas draining to the coast from the Clarence River at the easternmost edge of the NSA (69.642883°N, −140.978058°W) west to Point Barrow near Utqiagvik, Alaska (Figure 1). A total of 1,039 grid cells represent outlets along the domain's Alaska Beaufort Sea coast, hereafter referred to as “drainage outlets.” At 1 km resolution across the NSA, many of the outlets drain very small coastal catchments, often best represented by a single grid cell at the land-water interface. The lack of channelized flow and presence of direct groundwater inputs highlights the importance of capturing accurate surface and subsurface contributions to export on a cell-by-cell basis.

Table 1
Data Used in the PWBM Model Simulation and Validation

Variable	Period	Source
Air temperature	Daily	Daymet v4
Precipitation	Daily	Daymet v4
Wind speed	Daily	ECMWF Reanalysis v5
Surface water	Static	U.S. Geological Survey, National Hydrography Dataset (2024)
Landcover	Static	North American Land Change Monitoring System and National Land Cover Data set
Soil organic carbon	Static	Northern Circumpolar Soil Carbon Database v2
Soil organic carbon	Static	SoilGrids v2
Soil texture	Static	SoilGrids v2
Active layer thickness (ALT)	Average	National Tibetan Plateau/Third Pole Environment Data Center (TPDC); (Rawlins & Karmalkar, 2024)
River discharge	Daily	U.S. Geological Survey
DOC concentration	Average	Various sources

Note. Daily model forcings are for the period 1980–2023. Static model parameterization data are time-invariant in the simulation. Average listed for ALT and DOC concentration time period are calculated over several years. Sources are listed in the Data Availability statement.

2.2. Model Process Representations, Parameterizations and Forcings

Estimates of river discharge and DOC export were derived from a model simulation of the Permafrost Water Balance Model (PWBM) that was calibrated and validated using measured concentrations of DOC from a variety of northern Alaska streams and rivers reported by McClelland et al. (2014), Khosh (2015), Connolly et al. (2018), and Beaufort Lagoon Ecosystems LTER (2025). We use the PWBM version 4 (Rawlins et al., 2021; Rawlins & Karmalkar, 2024) to obtain outputs of runoff and DOC leaching and loading to river network segments for each of the $N = 166,483$ domain grid cells. The PWBM is an implicit daily time step model that includes physical process representations for snow accumulation and melt, soil active-layer development, DOC production and leaching, and other key processes that influence river discharge and DOC export. Subsurface runoff is modeled using a linear reservoir method, wherein the reservoirs are individual soil layers, with 10% of any amount above field capacity contributing to subsurface runoff. The sum total of subsurface and surface runoff enters the river network and becomes river freshwater volume. Additional details of model parameterization and configuration (e. g., vertical water fluxes, soil freeze-thaw and active layer dynamics) are described in Rawlins et al. (2021); Rawlins and Karmalkar (2024) and the technical description (Supporting Information S1).

The DOC parameterization routines within the PWBM were first described in Rawlins et al. (2021). Updates to extend the model to the finer 1 km spatial resolution are detailed in Supporting Information S1. Comprehensively simulating soil DOC production and desorption process is crucial in areas where water availability is substantial (Wei et al., 2024). In the PWBM, the leaching of DOC from soil occurs from a soil water DOC pool that is modulated by DOC production and decomposition as a function of soil organic carbon (SOC) density, soil temperature, and soil moisture. Production of DOC in a model soil layer or at the surface is influenced by the amount of available soil carbon and the temperature and moisture of each soil layer. The PWBM simulation analyzed in this study includes new data sets and associated parameterizations for soil and vegetation properties (Table 1).

Discharge volumes (from runoff) and DOC mass flux estimates for each grid cell are obtained from the core PWBM model, with routing performed in an “offline” model run outside of the core PWBM simulation. We found through testing and visual analysis of the simulated hydrographs that subdaily time steps are needed to move water and DOC mass through the relatively small 1 km^2 cell size network. In other words, water moves across several grid cells each day on its way downstream to the coast. Water volume and DOC mass movement across a constant $N = 14$ grid cells was chosen to simplify model calibration and validation. Efficacy in the simulated hydrographs is demonstrated through comparisons with observed data in Section 3.1. Simulated daily

DOC concentration is estimated as the product of DOC mass (milligrams) and water volume (liters), and is primarily used here for model evaluation against available data sampled from rivers. Lastly, inputs to coastal features, such as lagoons, bays and sounds are estimated from the quantities exiting each of the 1,039 drainage outlets bordering the northern coast.

Time varying meteorological data for precipitation, air temperature, and wind speed at standard 2 m height for the 44-year period 1980–2023 represent the primary controls on snow accumulation and melt, and the subsequent river discharge flux to the northern coast. We use Daymet version 4 data for daily precipitation and air temperature (Thornton et al., 2021) and ERA5 data for wind speed (Hersbach et al., 2020) (Table 1). Daymet is a 40-year daily meteorological data set on a 1 km grid for North America, Hawaii, and Puerto Rico and provides temperature, precipitation, shortwave radiation, vapor pressure, snow water equivalent, and day length. Version 4 represents several improvements from previous versions. The relatively coarse 31 km resolution ERA5 wind data were downscaled to each 1 km grid using nearest cell assignments, and we note that the lower spatial resolution potentially influences modeled snow densities (Rawlins et al., 2013). Landcover parametrizations were specified from the North American Land Change Monitoring System, with surface water from the United States Geological Survey's National Hydrography Data set.

2.3. Evaluation Data

To assess model performance, simulated active-layer thickness (ALT), river discharge, and river DOC concentrations are evaluated against independent data sets. Model estimates of river discharge are compared to measured data from United States Geological Survey (USGS) gauges. Among the large NSA rivers, only the Kuparuk River (USGS ID 15896000) has discharge data available for the entire study period. More limited data for the Canning River (USGS ID 15955000) from 2009 to 2012 and the Colville River (USGS ID 15875000) since 2003 are also available and are used to validate simulated river discharge. The gauge site on the Kuparuk is near the coast. The site on the Canning is approximately 40 km from the coast, while the site on the Colville is at Umiat, AK, well upstream (170 km). The Canning and Colville sites capture flow from 92.4% to 60.4% of each river's full contributing area, respectively.

Simulated end-of-season ALT estimates are evaluated against data derived from field measurements (Ran et al., 2022) and prior PWB simulations (Rawlins & Karmalkar, 2024). The ALT data from Ran et al. (2022) represent an integration of large amounts of ground and multisource geospatial data, especially remotely sensed data, synthesized through statistical learning modeling with an ensemble strategy. The prior model estimates are derived from simulations forced with three reanalysis data sets and the outputs from two global climate models. Gridded data from model output fields of the simulations forced with the six data sets represent a range of ALT that we compare to the simulation in this study. To accomplish this we extracted the grid cells over the NSA from the pan-Arctic simulation outputs described in Rawlins and Karmalkar (2024).

For model DOC validation we leverage field-collected measurements of DOC concentration gathered from a wide range of streams and rivers across the NSA. Downstream DOC data sets are most extensive for the Colville, Kuparuk, and Sagavanirktok rivers, but this study also takes advantage of several smaller data sets from other river outlets that expand the spatial extent and provide seasonal snapshots that can be validated across the NSA. In addition, a plethora of DOC data from river subbasins are included for model validation at smaller catchment scales (Connolly et al., 2018; Khosh et al., 2017; Koch et al., 2024).

3. Evaluation of Simulated Dynamics

The PWB simulation simulates an array of fundamental elements of the Arctic hydrological cycle. We focus our evaluation on river runoff, ALT, and DOC concentration given their importance in accurately estimating river discharge and DOC export magnitudes and temporal changes. Surface and subsurface runoff integrated across drainage areas via river routing becomes the estimate of river discharge at the coast. The seasonal progression of ALT has a bearing on the availability of SOC at various depths in the soil profile, and its trend over time influences the amount of SOC that can potentially be mobilized and transported through river networks to the coast. The concentration of DOC leached from soils and carried by rivers is fundamental to the estimation of DOC mass export. Through examination of the amounts and dynamics of these model variables, we establish the model's ability to capture key processes essential to simulation estimates of river discharge volumes and DOC export mass totals.

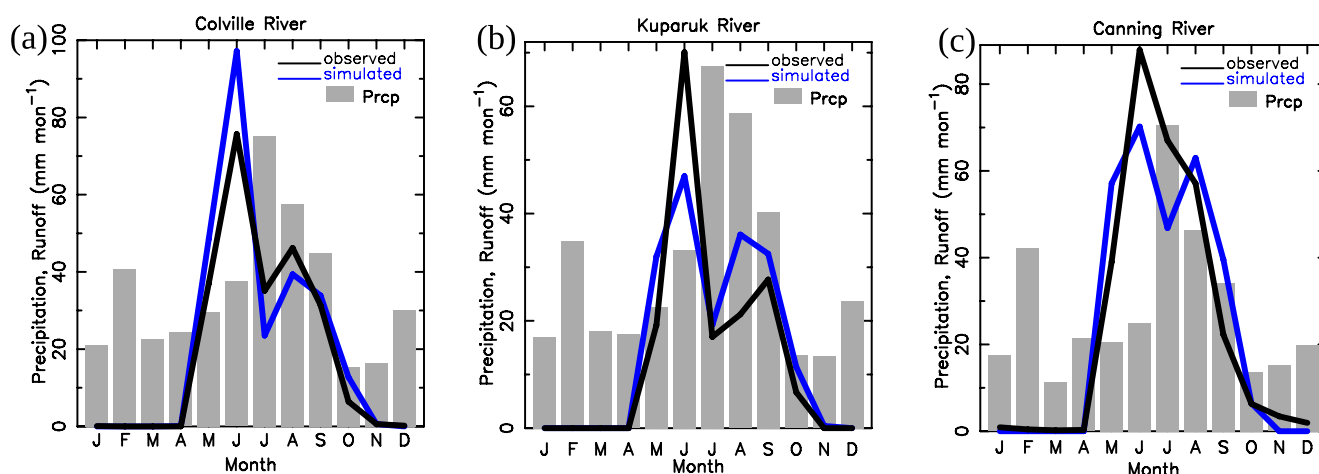


Figure 2. Monthly simulated precipitation, simulated runoff, and observed runoff as long-term averages over the Colville, Kugaruk, and Canning river basins. Simulated precipitation and runoff averages are for the period 2000–2023. Observed values are for the observational period of record for each gauge location.

3.1. River Runoff

Simulated river runoff is compared to measured records for the Colville, Kugaruk, and Canning rivers to ascertain model efficacy in estimating the magnitude and temporal variations in land-ocean river discharge flux. Observed and simulated runoff is derived from discharge volume by normalizing to (dividing by) basin area. Measured runoff is obtained from published discharge volume. For the validation comparisons we derive simulated runoff from simulated routed discharge, rather than simple average basin runoff, as it better captures the timing of peak discharge at the coast. Our analysis reveals that the model broadly captures the timing and magnitude of the spring freshet and summer baseflow conditions (Figure 2). Annual total runoff is within $\pm 11\%$ for each of the three rivers (Table 2). Simulated and measured annual runoff for the Colville is 256 and 233 mm yr^{-1} respectively, a difference (simulated minus observed) of -9.9% . Percent differences for the Kugaruk and Canning are $+10.9\%$ and -0.9% respectively. Peak discharge is slightly overestimated for the Colville and underestimated for the Kugaruk and Canning, suggesting an unbiased simulation for the NSA as a whole. This result is well supported by the relatively good performance for annual total runoff across the three rivers.

3.2. Active Layer Thickness

Simulated end-of-season ALT exhibits a spatial gradient with shallower ALT near the coast and deeper ALT in the Brooks Range, a pattern largely attributable to model parametrized thermal conductivities of soils, with more organic matter in the coastal plain tundra linked to lower conductivities and shallower ALT, and thinner organic soils in the mountains associated with higher conductivities and deeper ALT. Simulated ALT ranges from approximately 30 cm across the coastal plain tundra areas to just over 125 cm over parts of the central Brooks Range (Figure 3a). An isolated area of terrain in the easternmost region of Alaska has ALT reaching 150 cm. Deeper thaw depths across higher elevation terrains are attributable to less organic soil mass (e.g., peat), associated higher thermal conductivities, and thus more efficient downward propagation of surface energy.

Table 2
Annual Total Simulated and Observed Runoff (mm yr^{-1}) for the Colville, Kugaruk, and Canning River Basins

River	Simulated	Observed	Difference
Colville	256	233	-9.9
Kugaruk	180	162	10.9
Canning	284	286	-0.9

Note. Percent differences are calculated as $PD = (\text{simulated minus observed runoff})/\text{observed runoff}$.

Model simulated ALT is compared to ALT from a suite of data to assess model efficacy in capturing the magnitude of long-term average ALT across the NSA. A gridded product from the National Tibetan Plateau/Third Pole Environment Data Center (TPDC) (Ran et al., 2022) is used here, and represents a synthesis of observations. Based on this data, a majority of the region (50% between the 25th and 75th percentiles) has ALT between 45 and 73 cm (TPDC, Figure 3b). For ALT simulated in this study (Daymet*), 50% of the cell estimates are between 47 and 67 cm. Close correspondence is noted between the TPDC data and PWBM simulated estimates. The median of the TPDC observed and PWBM simulated distributions are 50 and 52 cm, respectively, and the means are 59 and 62 cm, respectively. The model

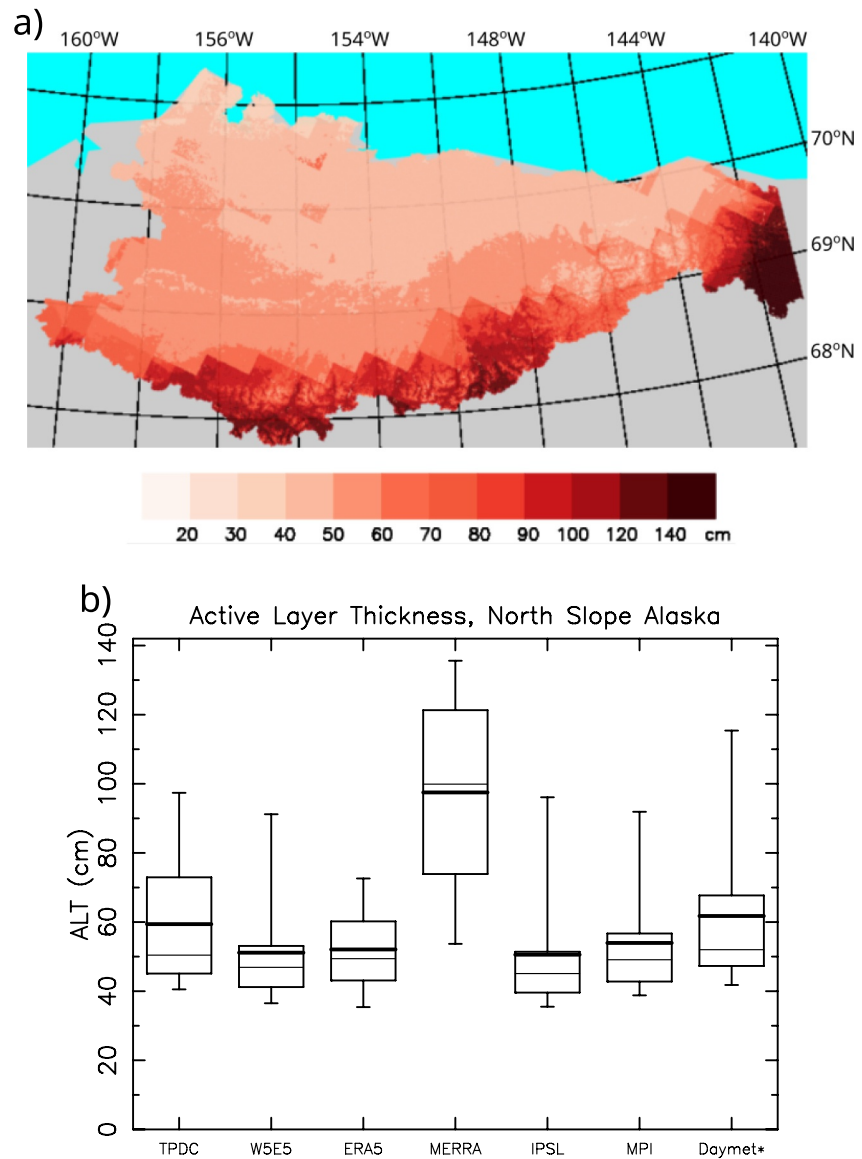


Figure 3. (a) End-of-season active-layer thickness from the PWBM simulation mapped as an average for the period 2000–2023. (b) Distributions of grid cell ALT across the NSA. Labels identify ALT drawn from observed data and PWBM simulations described in Rawlins and Karmalkar (2024) and this study, with the latter identified by forcing data set “Daymet*.” TPDC is a gridded data set based on ALT observations (Ran et al., 2022). Forcings W5E5, ERA5, MERRA are reanalysis data sets, and forcings IPSL and MPI represent outputs from global climate models (Rawlins & Karmalkar, 2024). Gridded ALT from TPDC are averages over the period 2000–2016, while the remaining estimates are averages for the period 2000–2019. Boxplot rectangles bracket the 25th and 75th percentiles. Whiskers extend to the 5th and 95th percentiles. Thick and thin horizontal lines mark the distribution mean and median respectively.

simulations from Rawlins and Karmalkar (2024) with five different forcings also provide a range of estimates to compare with the current Daymet* simulation. With the exception of the MERRA simulation, each has half of the distribution ALT values between 40 and 60 cm, comparable to the 44 and 58 from the present simulation. The PWBM has demonstrated efficacy in accurately replicating soil freeze-thaw dynamics and permafrost distribution at 1 km resolution in a Tibetan permafrost watershed characterized by a diverse range of soil properties including high gravel content and organic-rich mineral soils (Jiang et al., 2020, 2024). For example, simulated permafrost coverage was 75.9%, with coverage of 80.5% and 79.1% from two validation data sets, while simulated soil frozen ground coverage was 22.6%, with coverage of 19.3% and 20.9% in the validation data (Jiang et al., 2024).

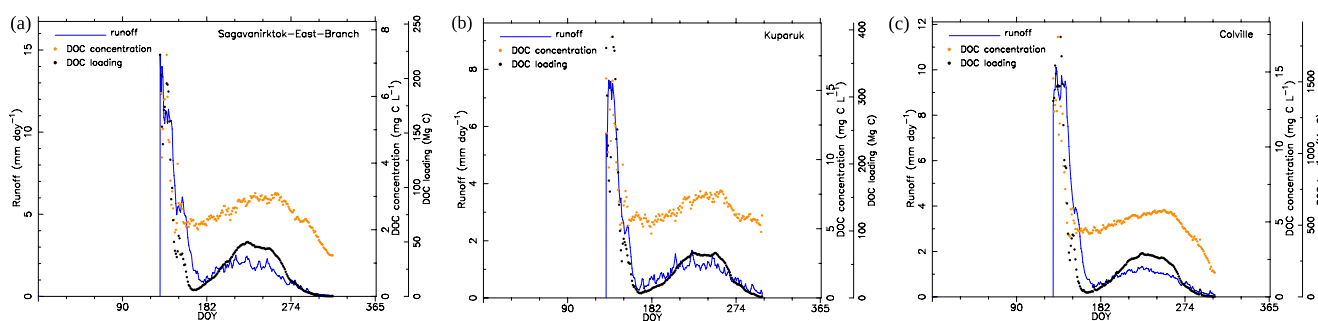


Figure 4. Simulated daily runoff, DOC concentration, and DOC loading as long-term averages over the Sagavanirktok, Kuparuk, and Colville rivers. The y axes are different in each figure panel.

Simulated ALT was also found to be unbiased in assessments against a series of field measurements in Alaska (Rawlins et al., 2013) and a gridded data set derived from observations ((Ran et al., 2022) used in this study) in an analysis spanning the pan-Arctic drainage basin (Rawlins & Karmalkar, 2024).

3.3. DOC Concentration

Simulated DOC concentrations for NSA subbasins and river outlets near the coast are compared to observed data to evaluate model efficacy in capturing DOC magnitudes, temporal dynamics, and spatial variations. We examine DOC concentrations and temporal dynamics here to assess model performance, particularly given the much finer spatial resolution applied in this study.

In recent years, estimates of DOC concentration for several of the region's larger rivers have been obtained through in situ sampling (Connolly et al., 2018; McClelland et al., 2014). Concentrations are highest during the spring, when water is constrained to shallow organic-rich flow paths, and decrease as the active layer extends into soils with greater mineral content and lower organic matter stocks (Khosh et al., 2017). Daily basin average simulated DOC concentrations for the Sagavanirktok, Kuparuk, and Colville rivers show this familiar pattern (Figure 4). Among the three rivers, the Sagavanirktok has the lowest DOC concentration, peaking at 6–7 mg C L⁻¹ during the freshet and averaging 2–3 mg C L⁻¹ through summer. Seasonal patterns in simulated DOC concentrations are similar for the Kuparuk and Colville, with average concentrations exceeding 15 mg C L⁻¹ in just a few days during the freshet. Summer values for the Colville and Kuparuk decrease to 5 mg C L⁻¹. These estimates are broadly consistent with measured data for the three rivers (McClelland et al., 2014) that also exhibit peak values during the freshet. The observations of McClelland et al. (2014) revealed freshet values for the Sagavanirktok of 8 mg C L⁻¹ and summer values of 1–3 mg C L⁻¹. For the Kuparuk, the measurements captured freshet values of around 14 mg C L⁻¹, 6 mg C L⁻¹ 40 days after peak freshet flow, and a few values of 3–4 mg/L 80 days after the freshet. Observations for the Colville showed concentrations at 2–3 mg C L⁻¹ a week before peak flow, rising to 11 mg C L⁻¹ at peak, and declining to 3–5 mg C L⁻¹ through summer.

The model's ability to capture spatial variations in DOC concentration across a broader extent of the NSA is assessed by comparing observational data for several dozen NSA subbasins and river outlets near the Beaufort Sea coast (35 with spring data, 81 summer data). A subbasin is defined here as an upstream contributing drainage area of a given river defined by a sampling site on that river network. Over all available subbasins, simulated DOC concentrations for spring (May–June) and summer (July–September) reveal a significant ($p < 0.001$) correlation with observed concentrations, with a Pearson's correlation coefficient of $r = 0.51$ (Table 3, Figure 5a). Many of the subbasins are relatively small: 37% of catchments with summer DOC data have a contributing area <100 km². The average error (simulated minus observed) for spring is -0.14 mg C L⁻¹ and the average error for summer is -1.29 mg C L⁻¹. For the outlet sites, the correlation is $r = 0.75$, the average error in spring is 1.72 mg C L⁻¹, and the average error in summer is 1.06 mg C L⁻¹

Table 3

Correlation Coefficient for Simulated and Observed DOC Concentrations for All NSA River Subbasins With Observed Seasonal Concentration Data and for the Subset of River Outlets, and Partitioned by Spring and Summer, the Average Error (AE, mg C L⁻¹), Mean Absolute Error (MAE, mg C L⁻¹) and Median Absolute Percentage Error (MPE, %)

	R	Spring			Summer		
		AE	MAE	MPE	AE	MAE	MPE
All subbasins	0.51	-0.14	1.9	67.2	-1.29	2.9	46.2
Coastal outlets	0.75	1.72	2.4	23.7	1.06	2.2	36.6

Note. Statistics are derived from the data values shown in Figure 5.

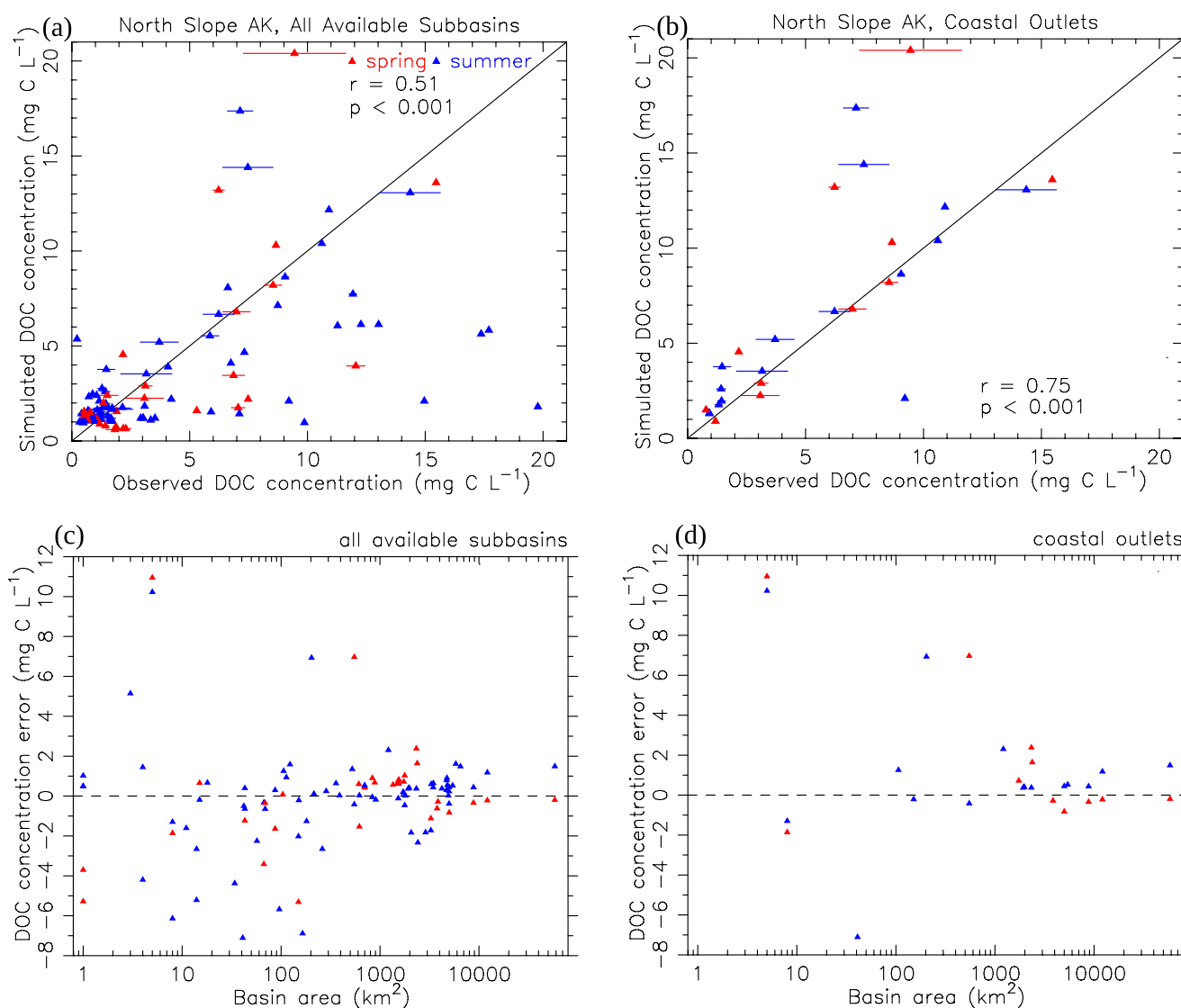


Figure 5. Spring (red) and summer (blue) simulated and observed DOC concentrations for (a) all NSA river subbasins with observed seasonal concentration data and (b) the subset of river outlets from (a). Spring and summer are defined as the average values for May–June and July–September respectively. Averaging periods for the observations vary (see methods). Simulated concentration averages are for the period 2000–2023. For observations with sufficient data, the horizontal line spans the 1 standard deviation range across each average value. Errors for (c) all subbasins and (d) the river outlets plotted against drainage basin area.

(Figure 5b). The residual between simulated and measured DOC concentrations are clearly highest for small basin sizes (Figures 5c and 5d). Put another way, errors are inversely proportional to catchment area, where most catchments with areas greater than 100 km² have errors less than 2 mg C L⁻¹ (47.6% of observed mean). For basin areas >3,000 km², the residual is less than 2 mg C L⁻¹ for all rivers. When comparing concentrations for river outlets at the coast, the clear outliers are four rivers with relatively small basin sizes of 5, 41, 203, and 549 km². River sampling was typically not made continuously throughout a season, with exception of six subbasins in the headwaters of the Kuparuk and Sagavanirktok (Khosh et al., 2017). In addition to basin size, errors may also be influenced by the number of repeated measurements averaged for a given site and season. In some cases, only a single measurement was used to compare to the simulated seasonal average. Thus, our validation of DOC at the subbasin scale is not expected to be as robust compared to the basin outlet evaluation that integrates larger drainage areas, and may include more seasonally explicit measurements with average values that better capture true seasonal means.

Table 4

Simulated Annual Total River Discharge ($\text{km}^3 \text{yr}^{-1}$), DOC Export (Mg yr^{-1}), Discharge Yield (mm yr^{-1}), and DOC Yield ($\text{g m}^{-2} \text{yr}^{-1}$) for the 10 Largest NSA Rivers (by Contributing Drainage Area) and for the Remaining NSA Terrestrial Drainage Areas

River	Contributing area km^2	River discharge ^a $\text{km}^3 \text{yr}^{-1}$	DOC export ^b Mg yr^{-1}	River yield ^c mm yr^{-1}	DOC yield ^d $\text{g m}^{-2} \text{yr}^{-1}$
Colville	59,647(36)	15.93(37)	50,997(31)	267.1	0.9
Ikpikpuk	15,215(9)	2.56(6)	19,287(12)	168.3	1.3
Sagavanirktok	13,465(8)	5.69(13)	8,515(5)	422.6	0.6
Meade	11,101(7)	2.81(7)	18,111(11)	253.1	1.6
Kuparuk	9,101(5)	2.23(5)	11,667(7)	245.0	1.3
Canning	5,414(3)	1.84(4)	2,164(1)	339.9	0.4
Fish	4,784(3)	0.61(1)	7,200(4)	127.5	1.5
Shaviovik	4,212(3)	1.02(2)	4,436(3)	242.2	1.1
Kongakut	3,875(2)	2.13(5)	1,087(1)	549.7	0.3
Topagoruk	3,199(2)	0.59(1)	4,327(3)	184.4	1.4
Other drainage areas	36,470(22)	7.40(17)	34,243(21)	185.0	1.1
Top 10 total	130,013(78)	35.42(83)	127,790(79)	272.4	1.0
All NSA total	166,483	42.82	162,033	257.2	1.0

Note. Totals are averages for the most recent 5-year period 2019–2023. Percentages (rounded to nearest integer) for each river contributing area and the percent contributions for river discharge and DOC export relative to the respective NSA totals are shown in parentheses (). ^aRiver total discharge volume. ^bRiver total DOC mass export. ^cRiver discharge divided by contributing drainage area. ^dRiver DOC export divided by contributing drainage area.

4. Results and Discussion

4.1. River Discharge and DOC Spatial and Temporal Dynamics

Total simulated river discharge from the NSA to the Beaufort Sea from 2019 to 2023 is $42.8 \text{ km}^3 \text{ yr}^{-1}$ (Table 4). As noted in previous studies, discharge from the Colville River is dominant: it accounts for $\sim 37\%$ of the total NSA river discharge, while the nine next largest drainage areas account for a combined $\sim 46\%$ of the total NSA discharge. Numerous smaller drainage areas account for the remaining 17%. DOC export from NSA rivers mirror their river discharge magnitudes, but variations in individual DOC yields due to differing amounts of mountain versus coastal plain terrain lead to some disproportionate DOC exports (Table 4). For example, the Ikpikpuk and Meade rivers each export roughly twice as much DOC as the Sagavanirktok River even though discharge from the Sagavanirktok is twice as high. Spatial patterns in DOC yield across the NSA reflect a west-east shift in drainage from greater landscape proportions of organic-rich foothills-tundra and coastal plain terrain (e.g., the Ikpikpuk, Meade, and Colville) to drainage from predominantly mountainous terrain (e.g., Sagavanirktok, Canning, Jago, and rivers to the east).

Simulated river DOC concentrations across the NSA reveal spatial variations that further elucidate patterns in DOC exports across the region. Concentrations are relatively low in the mountains and higher in the coastal plain (Figure 6). Peak (2-week) freshet DOC concentrations are less than 2 mg C L^{-1} in river sections draining higher elevation catchments in the Brooks Range, and exceed 15 mg C L^{-1} in river sections draining coastal plain tundra in northwestern catchments of the NSA (Figure 6a). The simulation captures the broad east-west gradient (east < west) and seasonal variations in concentrations (spring > summer) described in previous studies (Conolly et al., 2018; Rawlins et al., 2021) (Figure 6). The simulation also captures interesting spatial variations at smaller scales. For example, the simulation resulted in lower DOC concentrations locally in river corridors, a reflection of lower SOC amounts. Focusing in on areas that drain directly to coastal waters of the Deadhorse/Prudhoe Bay region (Figure 7), the simulation shows that DOC concentrations are much higher between the Colville and Kuparuk deltas than east of the Kuparuk to the Sagavnirktok. The lowest concentrations in this region are within the Sagavanirktok delta, a reflection of the delta's low SOC amounts parameterized from model input data. DOC-poor water in the east branch of Sagavanirktok, which accounts for a majority of its river

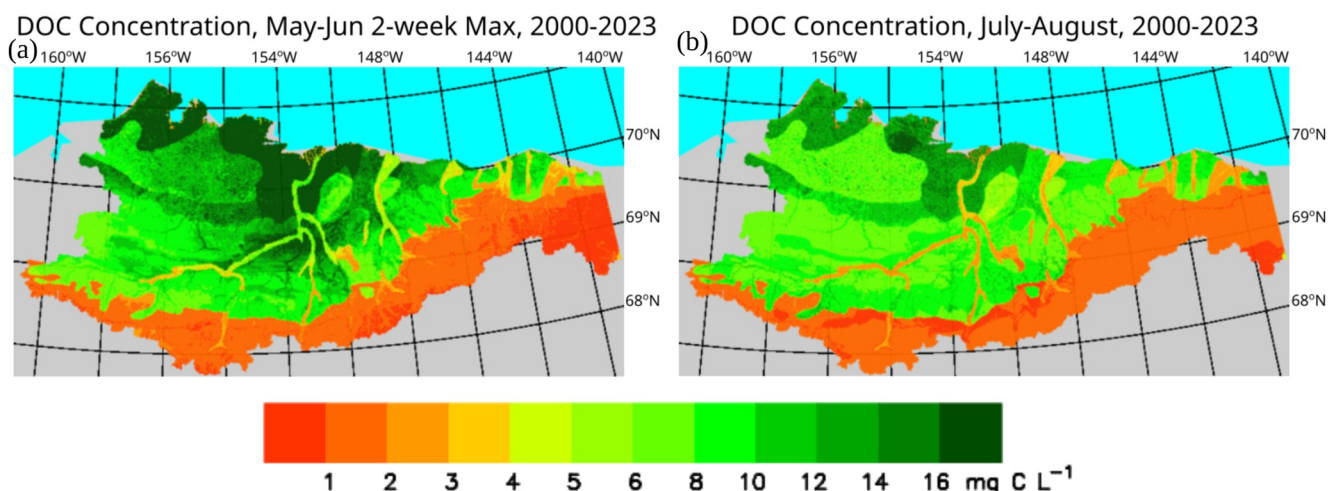


Figure 6. DOC concentrations of NSA river segments for (a) the maximum 2 weeks average during the freshet period (May–June) and (b) the July–August period average for the simulation. Soil SOC is parametrized with NCSCD v2 data (Hugelius et al., 2014). Values show are the climatological averages over years 2000–2023.

discharge, is attributable to its contributing basin draining a large proportion of the Brooks Range that contains relatively low SOC densities.

Although river discharge and DOC exports from the NSA as a whole can be accounted for by a few larger rivers, the biogeochemistry and ecology of individual estuaries along Alaska’s Beaufort Sea coast are strongly influenced by local inputs they receive. Thus, simulated inputs to select coastal water bodies were estimated to illustrate how DOC exports can be linked to and compared across coastal systems (Table 5). These include major named

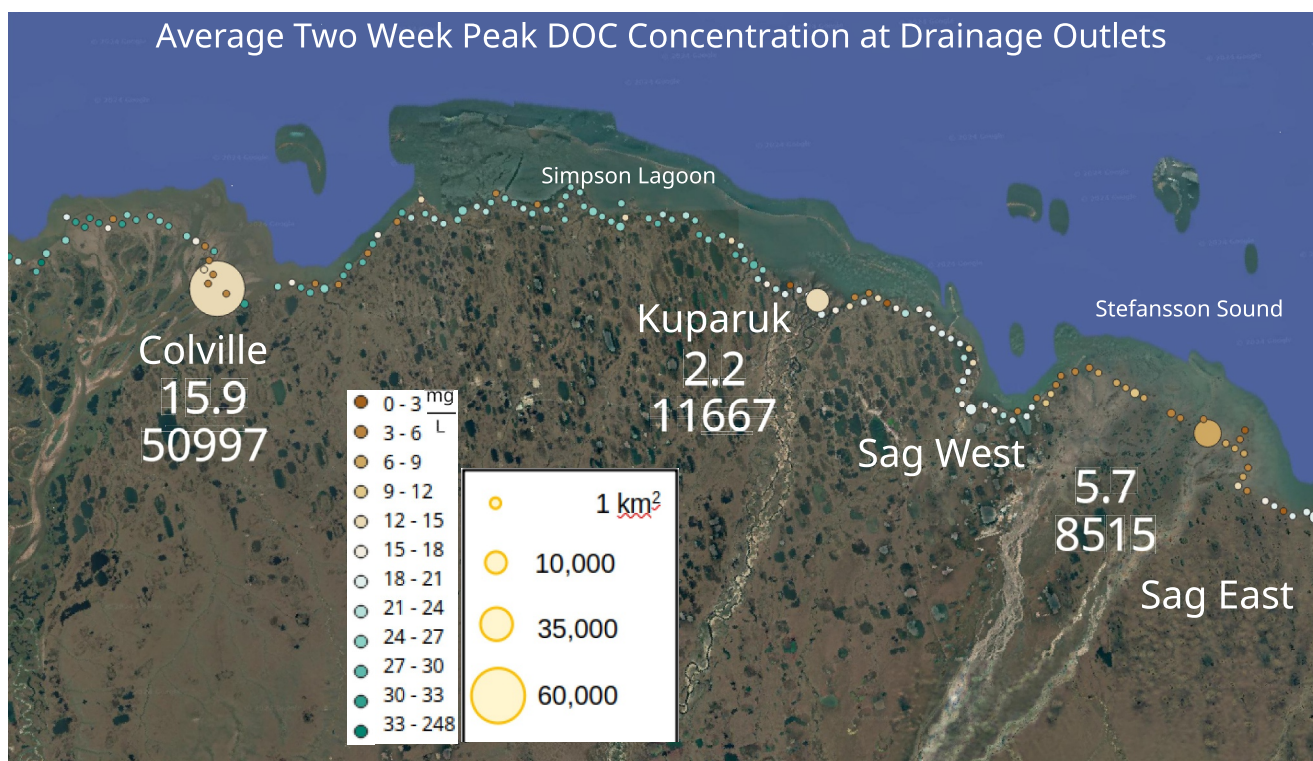


Figure 7. Maximum 2 weeks average (2000–2023) export DOC concentrations (colored circles, mg C L⁻¹) at drainage outlets in the Deadhorse/Prudhoe Bay region. Circle sizes scale by the respective river drainage area. Values below river names indicate river discharge (km³ yr⁻¹) and DOC export (Mg yr⁻¹) totals as averages for the period 2019–2023 (Table 4). For the Sagavanirktok, values represent the total flux for the east and west branches and the drainage areas between them.

Table 5
Simulated Annual Total River Discharge and DOC Export to Select NSA Coastal Features

Coastal feature	Feature area km ²	Contributing area km ²	River discharge ^a km ³ yr ⁻¹	River yield ^b mm yr ⁻¹	DOC export ^c Mg yr ⁻¹	DOC yield ^d g m ⁻² yr ⁻¹	Discharge normalized ^e km ³ km ⁻² yr ⁻¹	DOC normalized ^f Mg km ⁻² yr ⁻¹
Elson Lagoon	239.3	478	0.10	209	923	1.9	0.0004	3.7
Admiralty Bay	638.5	20,515	4.53	221	31,742	1.6	0.0071	49.7
Simpson Lagoon	273.6	10,415	2.42	232	13,851	1.3	0.0088	50.6
Stefansson Sound	883.8	20,295	7.20	355	16,313	0.8	0.0081	18.5
Kaktovik Lagoon	25.2	246	0.04	163	282	1.2	0.0016	11.2
Jago Lagoon	38.5	2387	0.66	277	1505	0.6	0.0171	39.1
Tapkaurak Lagoon	25.0	53	0.01	189	57	1.1	0.0004	2.3
Angun Lagoon	7.0	430	0.07	163	306	0.7	0.0100	43.6
Nuvagakpak Lagoon	30.6	1983	0.75	378	535	0.3	0.0245	17.5
Demarcation Bay	46.0	405	0.11	272	493	1.2	0.0024	10.7

Note. Export totals are averages for the 5-year period 2019–2023. Coastal features are ordered west to east. ^aRiver discharge volume from contributing drainage area into coastal feature. ^bRiver discharge volume divided by contributing drainage area. ^cDOC mass export from contributing drainage area into coastal feature. ^dDOC mass export divided by contributing drainage area. ^eRiver discharge volume entering coastal feature divided by feature area. ^fDOC mass export entering coastal feature divided by feature area.

lagoons, bays, and sounds along the coast, several of which are focal study areas of the Beaufort Lagoon Ecosystems (BLE) Long Term Ecological Research program (<https://ble.lternet.edu>) and have been investigated as a part of previous studies (Connolly et al., 2015; Dunton et al., 2012; Harris et al., 2018).

Discharge and DOC inputs to these receiving water bodies span roughly two orders of magnitude (Table 5). This wide range reflects differences in the size and geographic location of the land areas draining into them. Water and DOC inputs generally increase with contributing drainage area size, but DOC input yields (mass inputs divided by drainage area) decrease as proportional contributions from mountainous terrain increase. This pattern is attributable to landscape-linked variations in soil organic carbon content of the contributing areas draining to each estuary (Figure 8). Among the BLE focus estuaries, Elson Lagoon, which only receives drainage from the coastal plain, has the highest DOC input yield. Jago Lagoon, which receives most of its drainage from the Brooks Range, has the lowest DOC input yield. When normalized by the area of the receiving water body, on the other hand, discharge inputs are greatest to Nuvagakpak and Jago lagoons, whereas DOC inputs are greatest to Simpson Lagoon and Admiralty Bay.

While these results highlight geographic differences in water versus DOC yields across the NSA, they also remind us that the relative size of a receiving water body and associated drainage area matters. Terrestrial inputs have the greatest potential to influence coastal ecosystem processes where water from relatively large drainage areas is being funneled into relatively small receiving water bodies, and/or, where DOC yields are highest due to greater watershed proportions of SOC-rich terrain. Although not quantified in this study, differences in connectivity between estuarine water bodies and the open ocean also need to be considered. Greater connectivity and associated mixing between semi-enclosed estuaries and the open ocean reduces terrestrial influence potential, while the framing of barrier islands and the presence of narrow or few channels to the open ocean increases the residence time of terrestrial material.

4.2. River Flux Trends and Drivers of Change

Soil freezing and thawing influences the timing of DOC production, decomposition, and leaching in soils and its subsequent loading to river networks. The PWBM simulates soil freeze-thaw dynamics in detailed process representations, and in doing so facilitates an assessment of changes which influence river discharge and DOC exports. Simulated ALT exhibits trends over the simulation period that span an order of magnitude, from just under 0.05 cm yr⁻¹ to slightly over 0.5 cm yr⁻¹ across the NSA (Figure 9a). Higher thaw rates are evident in the Brooks Range and are modestly higher in the western as compared to the eastern part of the region. Enhanced thaw in mountainous terrain is attributable to a thinner organic layer, and thus higher thermal conductivity

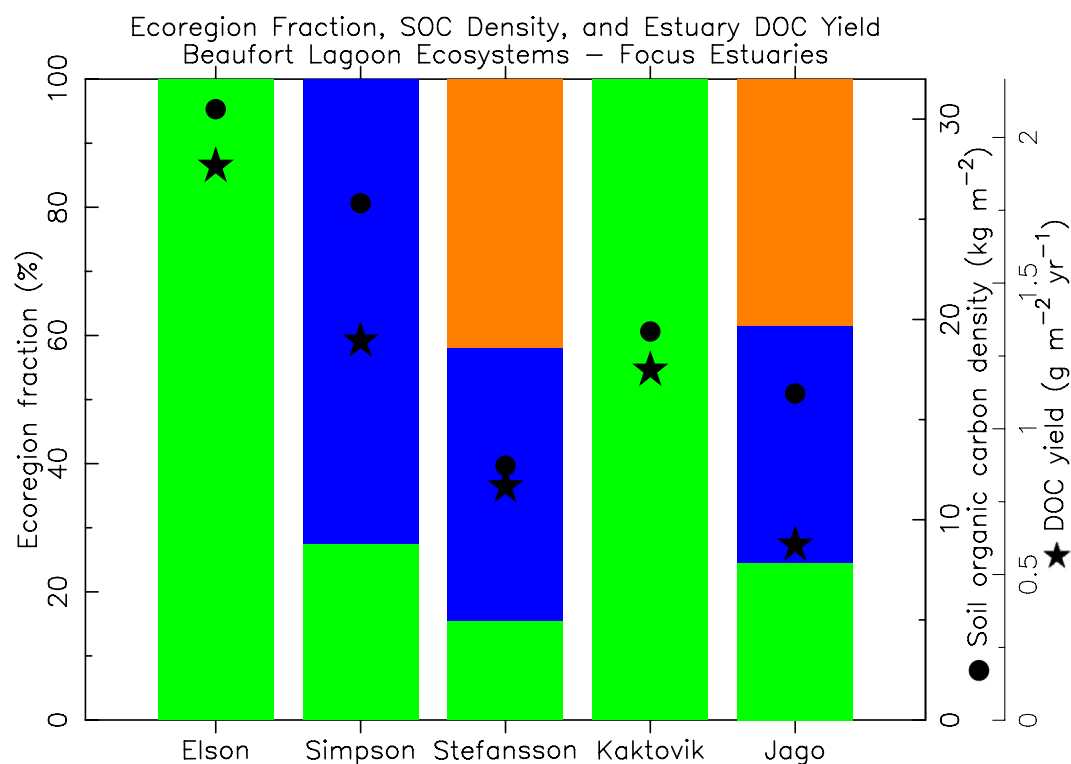


Figure 8. Ecoregion type (%), soil organic carbon density (kg m^{-2}), and DOC yield ($\text{g m}^{-2} \text{yr}^{-1}$) for BLE lagoons (and Stefansson Sound). Yield calculations are defined in Table 5. Values are averages across the contributing area draining to each water body for years 2019–2023. Water bodies are arranged from west to east (left to right).

between the surface and deeper mineral soils (Rawlins et al., 2019). Thawing has accelerated recently, with NSA domain median and mean ALT exceeding 68 and 86 cm, respectively, in both 2019 and 2023, compared to 46.6 and 54.7 cm, respectively, as averages over the years 1980–1989.

Permafrost thaw has the potential to mobilize previously frozen SOC and, in turn, contribute to increased DOC leaching and loading to river networks (Koch & O'Donnell, 2025). We used the time change in ALT for each domain grid cell, estimated by the linear least squares (LLS) fit over the simulation period, to estimate the amount of newly thawed SOC. The total mass of SOC thawed over the 44-year period was estimated by applying the vertical thickness of thawed soil onto the model parameterized (NCSCD) SOC. For example, if the LLS fit showed ALT deepening from 30 to 40 cm, the parameterized SOC in that depth range was calculated as the thawed C mass. We also estimated the total mass of thawed SOC using data from a second product (SoilGrids v2) (Poggio et al., 2021). The estimated thawed C mass ranges from 2 kg C in river valleys to as much as 20 kg C, primarily across the northern foothills of the Brooks Range (Figure 9b). Lower thawed C in river valleys are attributable to relatively low SOC densities, similar to their relatively low DOC concentrations (Figure 6). Higher thawed C amounts are attributable to higher SOC densities and/or greater rates of thaw. Intermediate thawed C amounts are evident across more northerly tundra areas, outside of the river valleys, due to both moderate permafrost thaw and higher SOC densities. Broadly speaking, the higher elevations of the Brooks Range have much lower thawed C mass compared to more northern areas. Similar amounts of thawed C mass are calculated when the ALT trend is applied to SoilGrids SOC data, with generally higher amounts over the northern Brooks Range foothills (Figure 9c). Notably, SoilGrids SOC data has non-zero SOC values across much of the Brooks Range, whereas the NCSCD data has many grid cells containing no SOC in those areas, and the thawed C amounts estimated from each data set reflect these differences.

Changes in monthly average runoff and DOC loading to rivers from both surface and subsurface contributions provide important insights into the seasonality of the river flux trends described below. Runoff in May more than doubled between the first 5 years (1980–1984) and the last 5 years (2019–2023) of the simulation period

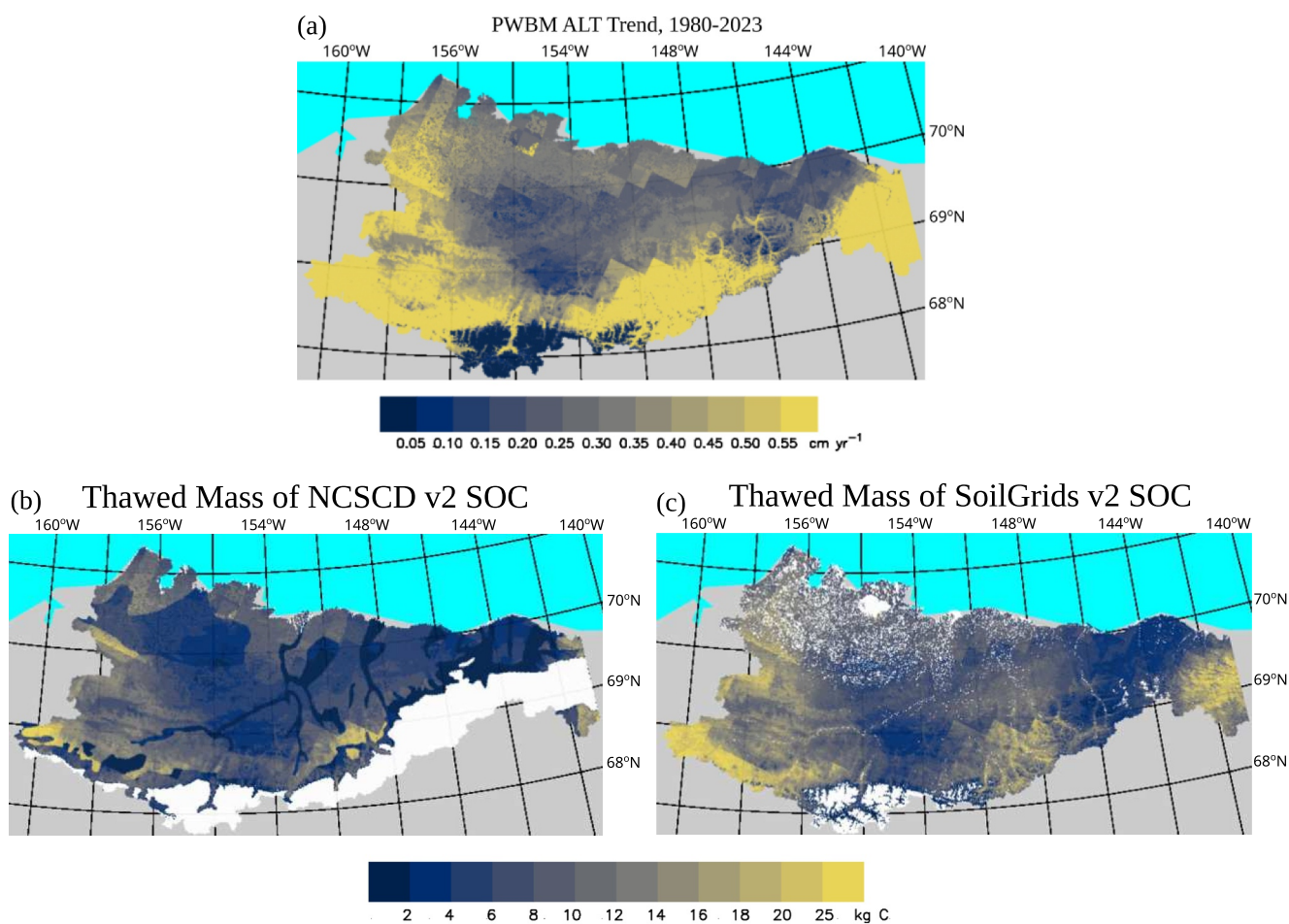


Figure 9. (a) Grid cell trend in active-layer thickness (ALT) from the simulation over the full simulation period 1980–2023. (b) Mass of SOC thawed over the same period for the baseline simulation parameterized with NCSCD SOC data. Thawed mass is estimated at each grid cell using ALT in the first and last years of the simulation as determined by the linear least squares regression fit to annual ALT. White shading represents areas with no valid SOC data, including water bodies and mountains. (c) Thawed mass as estimated by applying the simulated ALT trend to SoilGrids v2 SOC data.

(Figure 10a). This change is attributable to both an increase in simulated spring snow water equivalent, via hydrological cycle intensification, and a shift toward earlier snow melt from climate warming. June runoff decreased, due largely to the shift toward earlier snowmelt. In contrast, subsurface flow (supra-permafrost groundwater) during May was largely unchanged between the two periods. Capacity for subsurface flow is very limited during this time of year because the active layer is still largely frozen. Runoff increased during summer and autumn (July–October) through a rise in subsurface flow. DOC leaching and loading to river network segments increased in each month except June (Figure 10b). Loading in May increased by approximately 50%, primarily from DOC leaching and loading in surface flow, and a small subsurface contribution in the soil active layer. Sharp rises in DOC loading have occurred in late summer and autumn, with increases of 52%, 163%, 570% in August, September, and October respectively, attributable to increasing water availability (Arp et al., 2020; Rawlins, 2021) and increased loading via subsurface flow as a consequence of deepening ALT (Rawlins, 2021; St. Jacques & Sauchyn, 2009). This analysis highlights how inflows from surface runoff are the primary source of DOC, and likely, other river-borne nutrients to lagoons during spring (Grandi et al., 2025), with inputs from supra-permafrost groundwater becoming more important sources in summer and early autumn (Connolly et al., 2020; Demir et al., 2024).

Supra-permafrost groundwater flow at the land-sea interface supplies substantial quantities of DOC and nutrients directly to coastal waters, and thus represents an important energy source for coastal ecosystems (Connolly et al., 2020; Demir et al., 2024). Mean supra-permafrost groundwater flow rates were less than $\sim 55,000$ L yr⁻¹

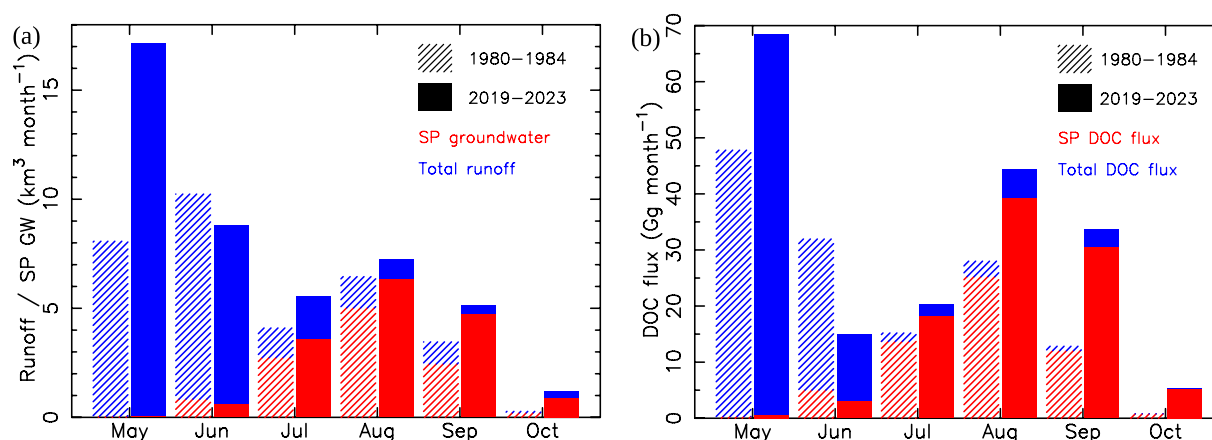


Figure 10. (a) Monthly average (red) supra-permafrost subsurface groundwater and (blue) total runoff ($\text{km}^3 \text{ yr}^{-1}$) to NSA river segments summed over all domain grid cells for the periods (hatched) 1980–1984 and (solid) 2019–2023. (b) Monthly average (red) supra-permafrost DOC flux and (blue) total DOC flux loaded to NSA river segments for the two 5-year periods.

(SD = 490 L yr^{-1}) before 1989, and have increased substantially over time, averaging $\sim 73,000$ (± 332) liters yr^{-1} from 2017 to 2023 (Figure 11). Supra-permafrost groundwater flow manifests greater interannual variability in recent years, with mean rates as high as $\sim 119,600$ (± 343) liters yr^{-1} in 2019 and as low as $\sim 23,500$ (± 307) liters yr^{-1} the following year. This increased variability may be related to hydrological cycle intensification (Arp et al., 2020; Magritsky et al., 2025; Rawlins et al., 2010) and permafrost thaw (Guimond et al., 2022; Rawlins, 2021; St. Jacques & Sauchyn, 2009). As the active layer deepens, the capacity to store and/or transport groundwater increases, leading to higher groundwater fluxes (less storage) in wet years and lower fluxes (more storage) in dry years. Accompanying this increase in freshwater flow, supra-permafrost DOC export to the Beaufort Sea has also increased. Mean rates were typically less than ~ 500 kg C yr^{-1} in the early 1980s and were more than ~ 845 kg C yr^{-1} in 2017, 2019, and 2023. Again, combined effects of hydrological cycle intensification and permafrost thaw could explain this trend. Corroborating our model results, simulated yields per kilometer of coastline are comparable to measured data from recent field sampling along shorelines of Kaktovik and Jago lagoons (Connolly et al., 2020).

Simulated river discharge and DOC export integrated across all NSA coastal outlets provide a means to synthesize changes that influence Beaufort Sea estuaries. River discharge increased significantly ($p < 0.01$) since 1980, rising from $\sim 30 \text{ km}^3 \text{ yr}^{-1}$ in the early 1980s to just over $45 \text{ km}^3 \text{ yr}^{-1}$ in the early 2020s (Figure 12). Three recent years—2018, 2019, 2023—have river discharge exceeding $60 \text{ km}^3 \text{ yr}^{-1}$, roughly double the flow that occurred during the early 1980s. DOC export also increased significantly, from $\sim 120 \text{ Gg C yr}^{-1}$ in the early 1980s to $\sim 170 \text{ Gg C yr}^{-1}$ in the early 2020s. DOC export exceeded 200 Gg C yr^{-1} in 2019 and 2023. Based on the LLS trend, river discharge increased at a rate of $0.33 \text{ km}^3 \text{ yr}^{-2}$, while DOC export increased by $1.15 \text{ Gg C yr}^{-2}$. The close coupling between annual discharge and DOC export is driven by the strong influence that water exerts on both DOC production in soils and the flushing events that load DOC to river networks (Connolly et al., 2018; Finlay et al., 2006; Kicklighter et al., 2013). The trend in DOC export is consistent with increased particulate organic carbon fluxes from pan-Arctic rivers between 1985 and 2022 attributed to increased precipitation and permafrost thaw (Sun et al., 2026).

Estimates of terrestrial DOC export reported in this study are essential for inventory assessments of carbon amounts in the Arctic Ocean (Kong et al., 2025), where limited observations render ocean CO_2 uptake rates highly uncertain (Dutch et al., 2025). Our focus on smaller coastal catchments is particularly important, as these systems are warming faster than the larger more southern-extending basins (Speetjens et al., 2023) which, in turn, is causing ground ice to melt in these flat coastal systems, sharply increasing hydrological drainage and further thaw (Liljedahl et al., 2016). Relatively high soil carbon stores in Arctic coastal catchments, along with the likelihood of future hydrological cycle intensification (Rawlins & Karmalkar, 2024), portends significant alterations to the biogeochemistry of coastal waters (Vonk et al., 2023). The increasing DOC exports may provide additional

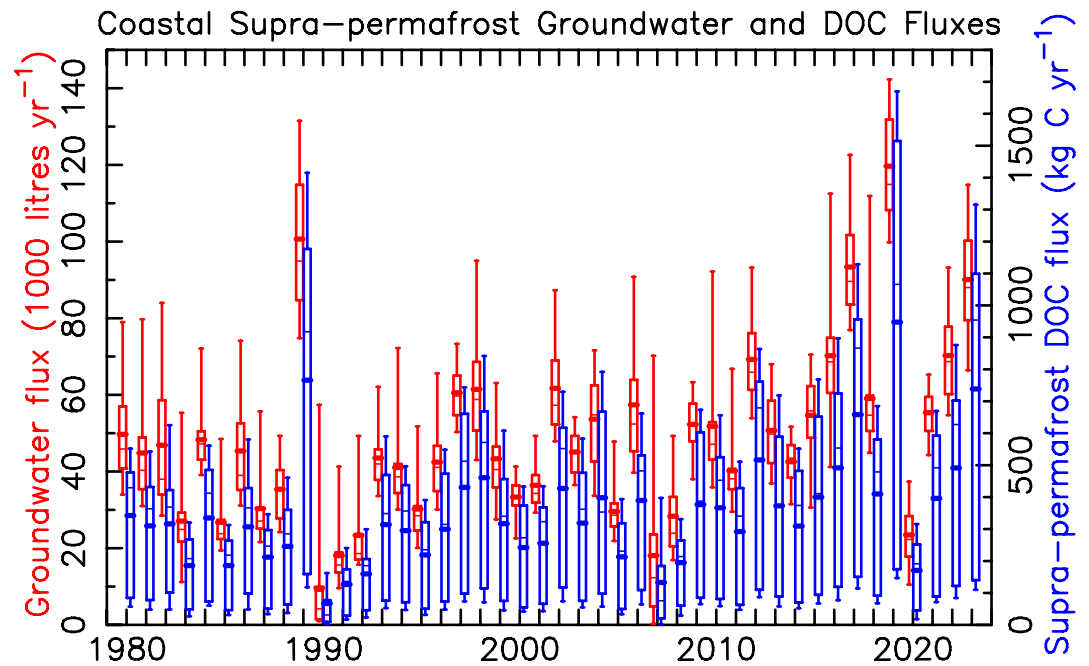


Figure 11. Annual total (red) supra-permafrost groundwater flux and (blue) supra-permafrost DOC flux for the 1,039 coastal drainage outlet cells. Simulated coastal supra-permafrost flows at the land-sea boundary are computed from daily subsurface runoff and DOC loading for each of the 1,039 drainage outlet cells.

Simulated Annual River Discharge and DOC Export, North Slope Drainage Area

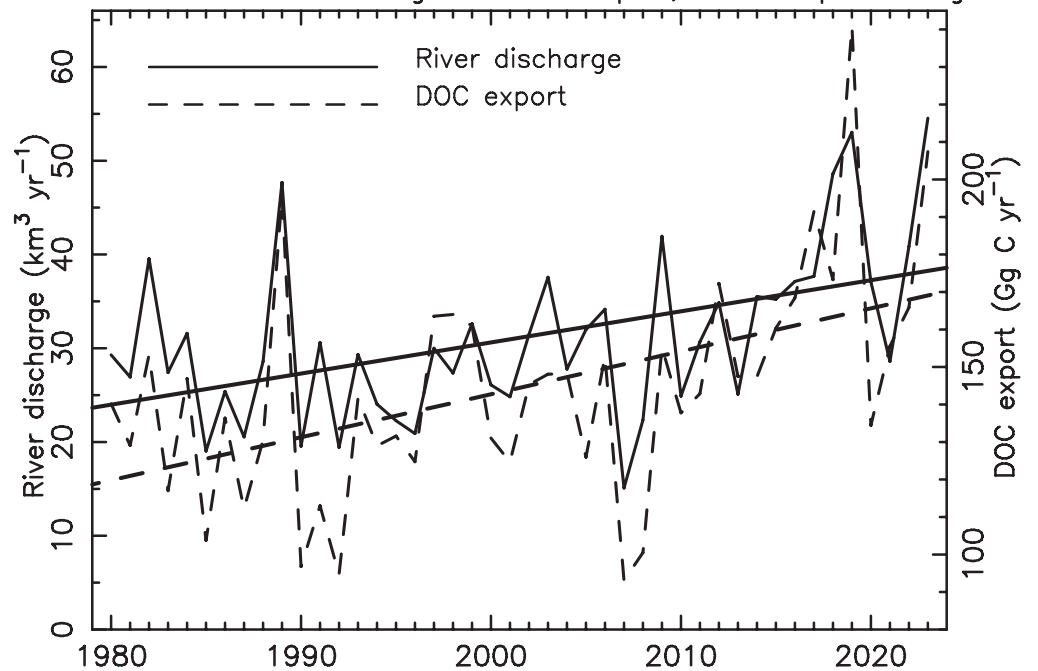


Figure 12. Annual total river discharge ($\text{km}^3 \text{ yr}^{-1}$) and DOC export (Gg C yr^{-1}) from all NSA drainage areas for the simulation period 1980–2023. Annual total river fluxes are sums from routed discharge and DOC mass and represent flows exiting from the domain's 1,039 coastal drainage outlets.

subsidies for food webs in Arctic coastal waters (Dunton et al., 2012; Harris et al., 2018; Stanek et al., 2024), while also potentially contributing to increased greenhouse gas emissions (Spera & Lougheed, 2025). Our analysis quantifies the amount of previously frozen SOC exposed through permafrost thaw (Schwab et al., 2020), a result with applicability in future modeling efforts, as recent studies have connected DOC age, its lability, and carbon respired by microbes in coastal waters (Mann et al., 2015; Rieb et al., 2024). Terrestrial fluvial models also hold the potential for offline and/or explicit connections to ocean biogeochemical models (Le Fouest et al., 2018; Undzisz et al., 2025) that are a vital component of interdisciplinary synthesis efforts focused on this sensitive region.

5. Conclusions

This study quantifies river discharge and DOC exports from NSA rivers to the Beaufort Sea coast and characterizes effects of climate change through the application of numerical process modeling. Runoff and DOC loading for the domain's 166,483 1 km² cells was routed through a digital river network to estimate the fluxes for 1,039 individual coastal outlets. Our modeling results reveal novel spatial and temporal patterns in river discharge, groundwater flow, and DOC export to estuaries that span the Alaskan Beaufort Sea coast in an environment where sparse observational data limits extrapolation to regional inputs.

Simulated daily climatological runoff and DOC concentrations for three NSA rivers reveal dynamics that have been shown in observational studies, namely high peak runoff and DOC concentrations during the spring freshet, lending confidence to the simulated flux totals across the domain. Estimates of contemporary inputs to specific coastal water bodies provide essential information that supports studies of ecosystem structure and function at the scale of individual lagoons, bays, and sounds along Alaska's Beaufort Sea coast. DOC inputs to lagoons near the western end of Alaska's Beaufort Sea coast are considerably higher than DOC inputs to lagoons at the eastern end, a pattern that reflects shifts in drainage from organic-rich tundra landscape in the west to mineral-soil-dominated alpine terrain to the east. The results demonstrate interplay between the size of a receiving water body and the size of the watershed draining into it. Terrestrial inputs have the greatest potential to influence coastal ecosystem processes when relatively large drainage areas funnel water and organic matter into relatively small lagoons. Consistent with previous studies (Arp et al., 2020; Rawlins et al., 2019), our results show that river discharge from the NSA to the Beaufort Sea is increasing and, moreover, point to rising supra-permafrost groundwater flows, mainly in late summer, and increasing DOC export to coastal waters.

Future modeling studies are needed to assess connections between river discharge, DOC export, and carbon cycling within coastal waters, particularly in lagoons and bays where barrier islands limit exchanges with the open seas. Model advances in partitioning between surface and subsurface contributions to DOC leaching would help to better understand how organic matter quality influences coastal ecosystems and their food webs. Adaptations of the PWBM that include other nutrient export modules (e.g., nitrogen) would also be valuable for evaluating linkages to coastal ecosystem dynamics. Future modeling efforts would benefit from investigations of the vertical movement of soil DOC and how it can be transformed during transport (He et al., 2025), as well as new data sets of temporally varying surface carbon parameterizations that account for changes in surface stocks and associated effects of climate warming. Field campaigns and remote-sensing approaches that quantify biogeochemical components of northern Alaska's coastal receiving bodies and adjacent waters will facilitate studies on the influence of river fluxes, climate change, and coastal ecosystems. For example, NASA's Arctic Boreal Vulnerability Experiment has produced a wealth of data useful for investigations of changing permafrost dynamics, disturbance regimes, and freshwater and DOC exports (Fisher et al., 2018; Miller et al., 2019). Our results demonstrate the importance of developing parsimonious, process-based models that simulate seasonal river discharges and DOC exports at the scale needed to create individual land-coastal system assessments. Furthermore, they highlight the variations in river discharge and DOC exports to northern Alaska's coastal estuaries, the effects of climate warming and change on the fluxes, and emphasize the need for dedicated field sampling activities, remote sensing observations, and model development efforts that will help to advance understanding of land-ocean connections in remote Arctic regions.

Conflict of Interest

The authors declare no conflicts of interest relevant to this study.

Data Availability Statement

All data used are available in the following references and sources. Daymet version 4 (Daymet: Daily Surface Weather Data on a 1-km Grid for North America, Version 4 R1, 2025) available at <https://doi.org/10.3334/ORNLAAC/2129>. European Centre for Medium-Range Weather Forecasts (European Centre for Medium-Range Weather Forecasts 2 m wind data, 2025) 2 m wind data available from <https://www.ecmwf.int/en/forecasts/dataset/ecmwf-reanalysis-v5-land>. Land cover data from the Alaska portion of the North American Land Change Monitoring System (North American Land Change Monitoring System, 2005) 2005 data set available from <https://catalog.snap.uaf.edu/geonetwork/srv/api/records/a370e48d-878c-41a2-add2-4e07479a5a95>. Surface water data for Alaska from the USGS National Hydrography Data set available from <https://www.usgs.gov/national-hydrography/nhdplus-high-resolution>. River discharge for the Canning River (USGS—Canning River, 2025) available from the USGS website at https://waterdata.usgs.gov/nwis/uv?site_no=15955000&legacy=1. River discharge for the Colville River (USGS—Colville River, 2025) available from the USGS website at https://waterdata.usgs.gov/nwis/uv?site_no=15875000&legacy=1. River discharge for the Kuparuk River (USGS—Kuparuk River, 2025) available from the USGS website at https://waterdata.usgs.gov/nwis/uv?site_no=15896000&legacy=1. Active layer thickness data from the National Tibetan Plateau Data Center in Ran et al. (2022). Soil organic carbon from the Northern Circumpolar Soil Carbon Database in Hugelius et al. (2013). Soil properties (SoilGrids 2.0) data in Poggio et al. (2021). Data from the model simulation, model source code, and associated files supporting the results are available at <https://doi.org/10.6073/pasta/03cdda13eb1af72787f8d7be848b9d34>.

Acknowledgments

This research was supported by grants from the U.S. National Science Foundation Division of Polar Programs NSF-OPP-2322664 and NSF-OPP-2234120, and the National Aeronautics and Space Administration Grant 80NSSC19K0649. The PWBM simulations were performed on high-performance computing resources provided by the Massachusetts Green High Performance Computing Center. The authors would like to thank the editor and three anonymous reviewers for their comments and suggestions that have helped us improve the final manuscript.

References

- Aagaard, K., & Carmack, E. C. (1989). The role of sea ice and other fresh waters in the Arctic circulation. *Journal of Geophysical Research*, *94*(C10), 14485–14498. <https://doi.org/10.1029/JC094iC10p14485>
- Arp, C., Whitman, M., Kemnitz, R., & Stuefer, S. (2020). Evidence of hydrological intensification and regime change from northern Alaskan watershed runoff. *Geophysical Research Letters*, *47*(17), e2020GL089186. <https://doi.org/10.1029/2020GL089186>
- Beaufort Lagoon Ecosystems LTER. (2025). Beaufort lagoon ecosystems LTER, core Program. 2025. In *Dissolved organic carbon (DOC) and total dissolved nitrogen (TDN) from river, lagoon, and open ocean sites along the Alaska Beaufort Sea coast, 2018-ongoing ver 11*. <https://doi.org/10.6073/pasta/e066f3043bb0968f6c56202e27572f59>
- Bense, V., Ferguson, G., & Kooi, H. (2009). Evolution of shallow groundwater flow systems in areas of degrading permafrost. *Geophysical Research Letters*, *36*(22), L22401. <https://doi.org/10.1029/2009GL039225>
- Bertin, C., Carroll, D., Menemenlis, D., Dutkiewicz, S., Zhang, H., Matsuoka, A., et al. (2023). Biogeochemical river runoff drives intense coastal Arctic Ocean CO₂ outgassing. *Geophysical Research Letters*, *50*(8), e2022GL102377. <https://doi.org/10.1029/2022GL102377>
- Brodzik, M. J., Billingsley, B., Haran, T., Raup, B., & Savoie, M. H. (2012). Ease-grid 2.0: Incremental but significant improvements for earth-gridded data sets. *ISPRS International Journal of Geo-Information*, *1*(1), 32–45. <https://doi.org/10.3390/ijgi1010032>
- Carmack, E. C., Yamamoto-Kawai, M., Haine, T. W., Bacon, S., Bluhm, B. A., Lique, C., et al. (2016). Freshwater and its role in the Arctic marine system: Sources, disposition, storage, export, and physical and biogeochemical consequences in the arctic and global oceans. *Journal of Geophysical Research: Biogeosciences*, *121*(3), 675–717. <https://doi.org/10.1002/2015JG003140>
- Clark, J. B., & Mannino, A. (2021). Preferential loss of Yukon River delta colored dissolved organic matter under nutrient replete conditions. *Limnology & Oceanography*, *66*(5), 1613–1626. <https://doi.org/10.1002/lno.11706>
- Clark, J. B., Mannino, A., Tzortziou, M., Spencer, R. G. M., & Hernes, P. (2022). The transformation and export of organic carbon across an Arctic river-delta-ocean continuum. *Journal of Geophysical Research: Biogeosciences*, *127*(12), e2022JG007139. <https://doi.org/10.1029/2022JG007139>
- Connelly, T. L., McClelland, J. W., Crump, B. C., Kellogg, C. T., & Dunton, K. H. (2015). Seasonal changes in quantity and composition of suspended particulate organic matter in lagoons of the Alaskan Beaufort Sea. *Marine Ecology Progress Series*, *527*, 31–45. <https://doi.org/10.3354/meps11207>
- Connolly, C. T., Cardenas, M. B., Burkart, G. A., Spencer, R. G., & McClelland, J. W. (2020). Groundwater as a major source of dissolved organic matter to Arctic coastal waters. *Nature Communications*, *11*(1), 1479. <https://doi.org/10.1038/s41467-020-15250-8>
- Connolly, C. T., Khosh, M. S., Burkart, G. A., Douglas, T. A., Holmes, R. M., Jacobson, A. D., et al. (2018). Watershed slope as a predictor of fluvial dissolved organic matter and nitrate concentrations across geographical space and catchment size in the Arctic. *Environmental Research Letters*, *13*(10), 104015. <https://doi.org/10.1088/1748-9326/aae35d>
- Daymet: Daily Surface Weather Data on a 1-km Grid for North America, Version 4 R1, 2025 Daymet: Daily Surface Weather Data on a 1-km Grid for North America, Version 4 R1. (2025). [Dataset]. <https://doi.org/10.3334/ORNLAAC/2129>
- Demir, C., McClelland, J. W., Bristol, E., Charette, M. A., & Cardenas, M. B. (2024). Coastal supra-permafrost aquifers of the arctic and their significant groundwater, carbon, and nitrogen fluxes. *Geophysical Research Letters*, *51*(22), e2024GL109142. <https://doi.org/10.1029/2024GL109142>
- Dunton, K. H., Schonberg, S. V., & Cooper, L. W. (2012). Food web structure of the Alaskan nearshore shelf and estuarine lagoons of the Beaufort Sea. *Estuaries and Coasts*, *35*(2), 416–435. <https://doi.org/10.1007/s12237-012-9475-1>
- Dutch, V. R., Bakker, D. C., Roobaert, A., Landschützer, P., Roden, N. P., Hoppema, M., & Kaiser, J. (2025). The Arctic Ocean CO₂ sink: Trends, uncertainties, and the impact of sea ice. *Global Biogeochemical Cycles*, *39*(8), e2025GB008576. <https://doi.org/10.1029/2025GB008576>
- European Centre for Medium-Range Weather Forecasts 2 m wind data. (2025). [Dataset]. Retrieved from <https://www.ecmwf.int/en/forecasts/dataset/ecmwf-reanalysis-v5-land>
- Fabre, C., Sonke, J. E., Tananaev, N., & Teisserenc, R. (2024). Organic carbon and mercury exports from pan-Arctic rivers in a thawing permafrost context—A review. *Science of the Total Environment*, *954*, 176713. <https://doi.org/10.1016/j.scitotenv.2024.176713>

- Finlay, J., Neff, J., Zimov, S., Davydova, A., & Davydov, S. (2006). Snowmelt dominance of dissolved organic carbon in high-latitude watersheds: Implications for characterization and flux of river DOC. *Geophysical Research Letters*, *33*(10), L10401. <https://doi.org/10.1029/2006GL025754>
- Fisher, J. B., Hayes, D. J., Schwalm, C. R., Huntzinger, D. N., Stofferahn, E., Schaefer, K., et al. (2018). Missing pieces to modeling the Arctic-Boreal puzzle. *Environmental Research Letters*, *13*(2), 020202. <https://doi.org/10.1088/1748-9326/aa9d9a>
- Gibson, G. A., Elliott, S. M., Piliouras, A., Kinney, J. L., & Jeffery, N. (2022). Assessing the potential impact of river chemistry on Arctic coastal production. *Frontiers in Marine Science*, *9*(675). <https://doi.org/10.3389/fmars.2022.738363>
- Grandi, G., Catalán, N., Bernal, S., Fasching, C., Battin, T. I., & Bertuzzo, E. (2025). Water transit time explains the concentration, quality and reactivity of dissolved organic carbon in an alpine stream. *Water Resources Research*, *61*(3), e2024WR039392. <https://doi.org/10.1029/2024WR039392>
- Guimond, J. A., Mohammed, A. A., Walvoord, M. A., Bense, V. F., & Kurylyk, B. L. (2022). Sea-level rise and warming mediate coastal groundwater discharge in the Arctic. *Environmental Research Letters*, *17*(4), 045027. <https://doi.org/10.1088/1748-9326/ac6085>
- Harris, C. M., McTigue, N. D., McClelland, J. W., & Dunton, K. H. (2018). Do high Arctic coastal food webs rely on a terrestrial carbon subsidy? *Food webs*, *15*, e00081. <https://doi.org/10.1016/j.fooweb.2018.e00081>
- He, Y., Hutchings, J. A., Assavanuvatt, P., Kanevskiy, M., Watts, E. G., Jones, B. M., et al. (2025). Inhibition of Arctic soil dissolved organic carbon export by the retention capacity of thawing permafrost. *Geophysical Research Letters*, *52*(24), e2025GL120418. <https://doi.org/10.1029/2025GL120418>
- Hersbach, H., Bell, B., Berrisford, P., Hirahara, S., Horányi, A., Muñoz-Sabater, J., et al. (2020). The ERA5 global reanalysis. *Quarterly Journal of the Royal Meteorological Society*, *146*(730), 1999–2049. <https://doi.org/10.1002/qj.3803>
- Holmes, R. M., McClelland, J. W., Peterson, B. J., Tank, S. E., Buluygina, E., Eglinton, T. I., et al. (2011). Seasonal and annual fluxes of nutrients and organic matter from large rivers to the Arctic Ocean and surrounding seas. *Estuaries and Coasts*, *35*(2), 369–382. <https://doi.org/10.1007/s12237-011-9386-6>
- Hugelius, G., Strauss, J., Zubrzycki, S., Harden, J. W., Schuur, E., Ping, C. L., et al. (2014). Estimated stocks of circumpolar permafrost carbon with quantified uncertainty ranges and identified data gaps. *Biogeosciences*, *11*(23), 6573–6593. <https://doi.org/10.5194/bg-11-6573-2014>
- Hugelius, G., Tarnocai, C., Broll, G., Canadell, J., Kuhry, P., & Swanson, D. (2013). The Northern Circumpolar Soil Carbon Database: Spatially distributed datasets of soil coverage and soil carbon storage in the northern permafrost regions. *Earth System Science Data*, *5*(1), 3–13. <https://doi.org/10.5194/essd-5-3-2013>
- Jiang, H., Yi, Y., Yang, K., Zhao, L., Chen, D., Kimball, J. S., et al. (2024). Soil freeze/thaw dynamics strongly influences runoff regime in a Tibetan permafrost watershed: Insights from a process-based model. *Catena*, *243*, 108182. <https://doi.org/10.1016/j.catena.2024.108182>
- Jiang, H., Yi, Y., Zhang, W., Yang, K., & Chen, D. (2020). Sensitivity of soil freeze/thaw dynamics to environmental conditions at different spatial scales in the central Tibetan plateau. *Science of the Total Environment*, *734*, 139261. <https://doi.org/10.1016/j.scitotenv.2020.139261>
- Kellogg, C. T., McClelland, J. W., Dunton, K. H., & Crump, B. C. (2019). Strong seasonality in Arctic estuarine microbial food webs. *Frontiers in Microbiology*, *10*, 2628. <https://doi.org/10.3389/fmicb.2019.02628>
- Khosh, M. S. (2015). *Seasonal dynamics of organic matter and inorganic nitrogen in surface waters of Alaskan Arctic streams and rivers* (Unpublished doctoral dissertation). University of Texas at Austin.
- Khosh, M. S., McClelland, J. W., Jacobson, A. D., Douglas, T. A., Barker, A. J., & Lehn, G. O. (2017). Seasonality of dissolved nitrogen from spring melt to fall freezeup in Alaskan Arctic tundra and mountain streams. *Journal of Geophysical Research: Biogeosciences*, *122*(7), 1718–1737. <https://doi.org/10.1002/2016JG003377>
- Kicklighter, D. W., Hayes, D. J., McClelland, J. W., Peterson, B. J., McGuire, A. D., & Melillo, J. M. (2013). Insights and issues with simulating terrestrial DOC loading of Arctic river networks. *Ecological Applications*, *23*(8), 1817–1836. <https://doi.org/10.1890/11-1050.1>
- Koch, J. C., Connolly, C. T., Repasch, M., Best, H. R., Couvillion, C. S., & Hunt, A. (2024). Hydrochemistry and age date tracers from springs, streams, and rivers in the Arctic national wildlife refuge, 2019–2022. *U.S. geological survey data release*. <https://doi.org/10.5066/P95CXJIT>
- Koch, J. C., & O'Donnell, J. A. (2025). Observing northern high-latitude river systems to understand changes in a warming Arctic. *Current Climate Change Reports*, *11*(1), 1–11. <https://doi.org/10.1007/s40641-025-00202-5>
- Kong, X., Lechtenfeld, O. J., Kaesler, J. M., Granskog, M. A., Stedmon, C. A., Graeve, M., & Koch, B. P. (2025). Major terrestrial contribution to the dissolved organic carbon budget in the Arctic Ocean. *Nature Geoscience*, *19*(1), 90–98. <https://doi.org/10.1038/s41561-025-01847-5>
- Le Fouest, V., Matsuoka, A., Manizza, M., Shernetsky, M., Tremblay, B., & Babin, M. (2018). Towards an assessment of riverine dissolved organic carbon in surface waters of the western Arctic Ocean based on remote sensing and biogeochemical modeling. *Biogeosciences*, *15*(5), 1335–1346. <https://doi.org/10.5194/bg-15-1335-2018>
- Liljedahl, A. K., Boike, J., Daanen, R. P., Fedorov, A. N., Frost, G. V., Grosse, G., et al. (2016). Pan-arctic ice-wedge degradation in warming permafrost and its influence on tundra hydrology. *Nature Geoscience*, *9*(4), 312–318. <https://doi.org/10.1038/ngeo2674>
- Liu, S., Kuhn, C., Amatulli, G., Aho, K., Butman, D. E., Allen, G. H., et al. (2022). The importance of hydrology in routing terrestrial carbon to the atmosphere via global streams and rivers. *Proceedings of the National Academy of Sciences*, *119*(11), e2106322119. <https://doi.org/10.1073/pnas.2106322119>
- Magritsky, D., Frolova, N., & Vasilenko, A. (2025). The inflow of river water into Russian Arctic seas: Its amount, long-term and intraannual changes. *Russian Meteorology and Hydrology*, *50*(5), 369–381. <https://doi.org/10.3103/S1068373925050012>
- Mann, P. J., Eglinton, T. I., McIntyre, C. P., Zimov, N., Davydova, A., Vonk, J. E., et al. (2015). Utilization of ancient permafrost carbon in headwaters of Arctic fluvial networks. *Nature Communications*, *6*(1), 7856. <https://doi.org/10.1038/ncomms8856>
- McClelland, J. W., Holmes, R. M., Dunton, K. H., & Macdonald, R. W. (2012). The Arctic Ocean Estuary. *Estuaries and Coasts*, *35*(2), 353–368. <https://doi.org/10.1007/s12237-010-9357-3>
- McClelland, J. W., Holmes, R. M., Peterson, B. J., Raymond, P. A., Striegl, R. G., Zhulidov, A. V., et al. (2016). Particulate organic carbon and nitrogen export from major Arctic rivers. *Global Biogeochemical Cycles*, *30*(5), 629–643. <https://doi.org/10.1002/2015GB005351>
- McClelland, J. W., Townsend-Small, A., Holmes, R. M., Pan, F., Stieglitz, M., Khosh, M. S., & Peterson, B. J. (2014). River export of nutrients and organic matter from the North Slope of Alaska to the Beaufort Sea. *Water Resources Research*, *50*(2), 1823–1839. <https://doi.org/10.1002/2013WR014722>
- Miller, C., Griffith, P., Goetz, S., Hoy, E., Pinto, N., McCubbin, I., et al. (2019). An overview of ABoVE airborne campaign data acquisitions and science opportunities. *Environmental Research Letters*, *14*(8), 080201. <https://doi.org/10.1088/1748-9326/ab0d44>
- Mohammed, A. A., Guimond, J. A., Bense, V. F., Jamieson, R. C., McKenzie, J. M., & Kurylyk, B. L. (2022). Mobilization of subsurface carbon pools driven by permafrost thaw and reactivation of groundwater flow: A virtual experiment. *Environmental Research Letters*, *17*(12), 124036. <https://doi.org/10.1088/1748-9326/aca701>
- North American Land Change Monitoring System. (2005). [Dataset]. Retrieved from <https://catalog.snap.uaf.edu/geonetwork/srv/api/records/a370e48d-878c-41a2-add2-4e07479a5a95>

- Poggio, L., de Sousa, L. M., Batjes, N. H., Heuvelink, G. B. M., Kempen, B., Ribeiro, E., & Rossiter, D. (2021). Soilgrids 2.0: Producing soil information for the globe with quantified spatial uncertainty. *SOIL*, 7(1), 217–240. <https://doi.org/10.5194/soil-7-217-2021>
- Ran, Y., Li, X., Cheng, G., Che, J., Aalto, J., Karjalainen, O., et al. (2022). New high-resolution estimates of the permafrost thermal state and hydrothermal conditions over the Northern Hemisphere. *Earth System Science Data*, 14(2), 865–884. <https://doi.org/10.5194/essd-14-865-2022>
- Rawlins, M. A. (2021). Increasing freshwater and dissolved organic carbon flows to northwest Alaska's Elson lagoon. *Environmental Research Letters*, 16(10), 105014. <https://doi.org/10.1088/1748-9326/ac2288>
- Rawlins, M. A., Cai, L., Stuefer, S. L., & Nicolsky, D. J. (2019). Changing characteristics of runoff and freshwater export from watersheds draining northern Alaska. *The Cryosphere*, 13(12), 3337–3352. <https://doi.org/10.5194/tc-13-3337-2019>
- Rawlins, M. A., Connolly, C. T., & McClelland, J. W. (2021). Modeling terrestrial dissolved organic carbon loading to western Arctic rivers. *Journal of Geophysical Research: Biogeosciences*, 126(10), e2021JG006420. <https://doi.org/10.1029/2021JG006420>
- Rawlins, M. A., & Karmalkar, A. V. (2024). Regime shifts in Arctic terrestrial hydrology manifested from impacts of climate warming. *The Cryosphere*, 18(3), 1033–1052. <https://doi.org/10.5194/tc-18-1033-2024>
- Rawlins, M. A., Nicolsky, D. J., McDonald, K. C., & Romanovsky, V. E. (2013). Simulating soil freeze/thaw dynamics with an improved pan-Arctic water balance model. *Journal of Advances in Modeling Earth Systems*, 5(4), 659–675. <https://doi.org/10.1002/jame.20045>
- Rawlins, M. A., Steele, M., Holland, M. M., Adam, J. C., Cherry, J. E., Francis, J. A., et al. (2010). Analysis of the Arctic system for freshwater cycle intensification: Observations and expectations. *Journal of Climate*, 23(21), 5715–5737. <https://doi.org/10.1175/2010JCLI3421.1>
- Rieb, E. C., Polik, C. A., Ward, C. P., Kling, G. W., & Cory, R. M. (2024). Controls on the respiration of ancient carbon draining from permafrost soils into sunlit Arctic surface waters. *Journal of Geophysical Research: Biogeosciences*, 129(5), e2023JG007853. <https://doi.org/10.1029/2023JG007853>
- Schwab, M. S., Hilton, R. G., Raymond, P. A., Haghpour, N., Amos, E., Tank, S. E., et al. (2020). An abrupt aging of dissolved organic carbon in large Arctic Rivers. *Geophysical Research Letters*, 47(23), e2020GL088823. <https://doi.org/10.1029/2020GL088823>
- Shogren, A. J., Zarnetske, J. P., Abbott, B. W., Grose, A. L., Rec, A. F., Nipko, J., et al. (2024). Hydrology controls dissolved organic carbon and nitrogen export and post-storm recovery in two Arctic headwaters. *Journal of Geophysical Research: Biogeosciences*, 129(2), e2023JG007583. <https://doi.org/10.1029/2023JG007583>
- Shogren, A. J., Zarnetske, J. P., Abbott, B. W., Iannucci, F., & Bowden, W. B. (2020). We cannot shrug off the shoulder seasons: Addressing knowledge and data gaps in an Arctic headwater. *Environmental Research Letters*, 15(10), 104027. <https://doi.org/10.1088/1748-9326/ab9d3c>
- Song, M., Huang, J., Zhao, D., & Mu, Y. (2025). Trends and drivers of dissolved organic carbon in major Arctic rivers. *Ecological Indicators*, 170(113081), 113081. <https://doi.org/10.1016/j.ecolind.2025.113081>
- Speetjens, N. J., Hugelius, G., Gumbrecht, T., Lantuit, H., Berghuijs, W. R., Pika, P. A., et al. (2023). The pan-Arctic catchment database (ARCADE). *Earth System Science Data*, 15(2), 541–554. <https://doi.org/10.5194/essd-15-541-2023>
- Spera, A., Peterson, S., Tweedie, C., & Loughheed, V. (2026). Wind-driven circulation impacts water quality and pCO₂ over an estuarine gradient in an Arctic lagoon. *Estuaries and Coasts*, 49(2), 49. <https://doi.org/10.1007/s12237-025-01662-6>
- Spera, A. C., & Loughheed, V. L. (2025). Carbon dioxide fluxes of Arctic coastal ecosystems controlled by seasonal patterns of land-to-ocean connectivity. *Limnology & Oceanography*, 70(8), 2175–2191. <https://doi.org/10.1002/lno.70101>
- Stanek, A. E., O'Donnell, J. A., Carey, M. P., Laske, S. M., Xu, X., Dunton, K. H., & von Biela, V. R. (2024). Arctic fishes reveal patterns in radiocarbon age across habitats and with recent climate change. *Limnology and Oceanography Letters*, 9(6), 796–805. <https://doi.org/10.1002/lo12.10442>
- Starr, S., Johnston, S. E., Sobolev, N., Perminova, I., Kellerman, A., Fiske, G., et al. (2023). Characterizing uncertainty in pan-Arctic land-ocean dissolved organic carbon flux: Insights from the Onega River, Russia. *Journal of Geophysical Research: Biogeosciences*, 128(5), e2022JG007073. <https://doi.org/10.1029/2022JG007073>
- St. Jacques, J. M., & Sauchyn, D. J. (2009). Increasing winter baseflow and mean annual streamflow from possible permafrost thawing in the Northwest Territories, Canada. *Geophysical Research Letters*, 36, L01401. <https://doi.org/10.1029/2008GL035822>
- Sun, X., Tian, L., Fang, H., Walling, D. E., Syvitski, J., Huang, L., et al. (2026). Mapping pan-Arctic riverine particulate organic carbon from space (1985 to 2022). *Science Advances*, 12(3), eady6314. <https://doi.org/10.1126/sciadv.ady6314>
- Tank, S. E., McClelland, J. W., Spencer, R. G., Shiklomanov, A. I., Suslova, A., Moatar, F., et al. (2023). Recent trends in the chemistry of major northern rivers signal widespread Arctic change. *Nature Geoscience*, 16(9), 789–796. <https://doi.org/10.1038/s41561-023-01247-7>
- Thornton, P. E., Shrestha, R., Thornton, M., Kao, S.-C., Wei, Y., & Wilson, B. E. (2021). Gridded daily weather data for North America with comprehensive uncertainty quantification. *Scientific Data*, 8(1), 190. <https://doi.org/10.1038/s41597-021-00973-0>
- Undzis, B., Moriarty, J. M., Eidam, E. F., & Overeem, I. (2025). The influence of wave events on open water suspended sediment fluxes on the Alaskan Beaufort Sea shelf: A numerical modeling study. *Journal of Geophysical Research: Oceans*, 130(12), e2025JC023043. <https://doi.org/10.1029/2025JC023043>
- USGS—Canning River. (2025). [Dataset]. Retrieved from https://waterdata.usgs.gov/nwis/uv?site_no=15955000&legacy=1
- USGS—Colville River. (2025). [Dataset]. Retrieved from https://waterdata.usgs.gov/nwis/uv?site_no=15875000&legacy=1
- USGS National Hydrography Dataset—surface water product. (2024). [Dataset]. Retrieved from <https://www.usgs.gov/national-hydrography/nhdplus-high-resolution>
- USGS—Kuparuk River. (2025). [Dataset]. Retrieved from https://waterdata.usgs.gov/nwis/uv?site_no=15896000&legacy=1
- Vonk, J., Speetjens, N., & Poste, A. (2023). Small watersheds may play a disproportionate role in arctic land-ocean fluxes. *Nature Communications*, 14(1), 3442. <https://doi.org/10.1038/s41467-023-39209-7>
- Vonk, J. E., Fritz, M., Speetjens, N. J., Babin, M., Bartsch, A., Basso, L. S., et al. (2025). The land-ocean arctic carbon cycle. *Nature Reviews Earth & Environment*, 6(2), 86–105. <https://doi.org/10.1038/s43017-024-00627-w>
- Walvoord, M. A., & Kurylyk, B. L. (2016). Hydrologic impacts of thawing permafrost—A review. *Vadose Zone Journal*, 15(6), vzt2016.01.0010. <https://doi.org/10.2136/vzt2016.01.0010>
- Wang, P., Huang, Q., Pozdniakov, S. P., Liu, S., Ma, N., Wang, T., et al. (2021). Potential role of permafrost thaw on increasing Siberian river discharge. *Environmental Research Letters*, 16(3), 034046. <https://doi.org/10.1088/1748-9326/abe326>
- Wei, X., Hayes, D. J., Butman, D. E., Qi, J., Ricciuto, D. M., & Yang, X. (2024). Modeling exports of dissolved organic carbon from landscapes: A review of challenges and opportunities. *Environmental Research Letters*, 19(5), 053001. <https://doi.org/10.1088/1748-9326/ad3cf8>

References From the Supporting Information

- Alexeev, V., Nicolovsky, D., Romanovsky, V., & Lawrence, D. (2007). An evaluation of deep soil configurations in the CLM3 for improved representation of permafrost. *Geophysical Research Letters*, 34(9). <https://doi.org/10.1029/2007GL029536>
- Andersland, O., & Anderson, D. (1978). *Geotechnical engineering for cold regions*. McGraw-Hill.
- Carslaw, H. (1959). *Conduction of heat in solids* (Vol. 302, pp. 340–341). Oxford University Press.
- Cory, R. M., Ward, C. P., Crump, B. C., & Kling, G. W. (2014). Sunlight controls water column processing of carbon in arctic fresh waters. *Science*, 345(6199), 925–928. <https://doi.org/10.1126/science.1253119>
- Dalhuijsen, A., & Segal, A. (1986). Comparison of finite element techniques for solidification problems. *International Journal for Numerical Methods in Engineering*, 23(10), 1807–1829. <https://doi.org/10.1002/nme.1620231003>
- DeVries, D. (1963). Thermal properties of soils. In *Physics of plant environment WR Van wijk*. North-Holland.
- Dolan, W., Pavelsky, T., Davis, J., LaFramboise, N., Polik, C., & Cory, R. (2025). Effects of total suspended solids on photomineralization of dissolved organic matter in the Peace-Athabasca Delta, Canada. *Journal of Geophysical Research: Biogeosciences*, 130(6), e2024JG008620. <https://doi.org/10.1029/2024JG008620>
- Federer, C. A., & Lash, D. (1978). *Brook: A hydrologic simulation model for eastern forests* (Tech. Rep.). University of New Hampshire Water Resources Research Center NH Water Resources Research Center Scholarship No. 119. Retrieved from https://scholars.unh.edu/nh_wrrc_scholarship/172
- Forouki, O. T. (1981). *Thermal properties of soils* (Tech. Rep.). (Report No. Vol. 81, No. 1, CRREL Monograph). CRREL.
- Global gridded surfaces of selected soil characteristics, 2000 Global gridded surfaces of selected soil characteristics (IGBPDIS). (2000). <https://doi.org/10.3334/ORNLDAAC/569>
- Global Soil Data Task. (2000). Global gridded surfaces of selected soil characteristics (IGBPDIS). <https://doi.org/10.3334/ORNLDAAC/569>
- Guo, L., & Macdonald, R. W. (2006). Source and transport of terrigenous organic matter in the upper Yukon River: Evidence from isotope ($\delta^{13}\text{C}$, $\delta^{14}\text{C}$, and $\delta^{15}\text{N}$) composition of dissolved, colloidal, and particulate phases. *Global Biogeochemical Cycles*, 20(2). <https://doi.org/10.1029/2005GB002593>
- Hamon, W. R. (1963). Computation of direct runoff amounts from storm rainfall. *International Association of Hydrological Sciences*, 63, 52–62.
- Hinzman, L. D., & Kane, D. L. (1991). Snow Hydrology of a Headwater Arctic Basin 2. Conceptual analysis and computer modeling. *Water Resources Research*, 27(6), 1111–1121. <https://doi.org/10.1029/91WR00261>
- Holmes, R. M., McClelland, J. W., Raymond, P. A., Frazer, B. B., Peterson, B. J., & Stieglitz, M. (2008). Lability of DOC transported by Alaskan rivers to the Arctic Ocean. *Geophysical Research Letters*, 35(3). <https://doi.org/10.1029/2007GL032837>
- Jackson, R., Canadell, J., Ehleringer, J. R., Mooney, H., Sala, O., & Schulze, E. D. (1996). A global analysis of root distributions for terrestrial biomes. *Oecologia*, 108(3), 389–411. <https://doi.org/10.1007/BF00333714>
- Lawrence, D. M., & Slater, A. G. (2008). Incorporating organic soil into a global climate model. *Climate Dynamics*, 30(2–3), 145–160. <https://doi.org/10.1007/s00382-007-0278-1>
- Liston, G. E., Haehnel, R. B., Sturm, M., Hiemstra, C. A., Berezovskaya, S., & Tabler, R. D. (2007). Simulating complex snow distributions in windy environments using SnowTran-3D. *Journal of Glaciology*, 53(181), 241–256. <https://doi.org/10.3189/172756507782202865>
- Lunardini, V. J. (1978). Theory of N-factor and correlation of data. In *Proceedings of the third international conference on permafrost* (Vol. 1, pp. 40–46). National Council of Canada.
- Lunardini, V. J. (1981). *Heat transfer in cold climates* (p. 731). Van Nostrand Reinhold.
- Mao, J., & Yan, B. (2019). *Global monthly mean leaf area index climatology, 1981-2015* (Tech. Rep.). ORNL DAAC. <https://doi.org/10.3334/ORNLDAAC/1653>
- McGuire, A. D., Hayes, D. J., Kicklighter, D. W., Manizza, M., Zhuang, Q., Chen, M., et al. (2010). An analysis of the carbon balance of the Arctic Basin from 1997 to 2006. *Tellus B: Chemical and Physical Meteorology*, 62(5), 455–474. <https://doi.org/10.1111/j.1600-0889.2010.00497.x>
- Monteith, J. L. (1965). Evaporation and environment. In G. E. Fogg (Ed.), *The State and movement of water in living organisms* (pp. 205–233). Cambridge University Press.
- Neff, J., Finlay, J., Zimov, S., Davydov, S., Carrasco, J., Schuur, E., & Davydova, A. (2006). Seasonal changes in the age and structure of dissolved organic carbon in Siberian Rivers and streams. *Geophysical Research Letters*, 33(23). <https://doi.org/10.1029/2006GL028222>
- Nicolovsky, D., Romanovsky, V., Alexeev, V., & Lawrence, D. (2007). Improved modeling of permafrost dynamics in a GCM land-surface scheme. *Geophysical Research Letters*, 34, L08501. <https://doi.org/10.1029/2006GL028222>
- Nicolovsky, D., Romanovsky, V., & Panteleev, G. (2009). Estimation of soil thermal properties using in-situ temperature measurements in the active layer and permafrost. *Cold Regions Science and Technology*, 55(1), 120–129. <https://doi.org/10.1016/j.coldregions.2008.03.003>
- Rawlins, M. A., Connolly, C. T., & McClelland, J. W. (2026). Hydrological cycle intensification and permafrost thaw drive increased freshwater and organic carbon inputs to northern Alaska estuaries. *Global Biogeochemical Cycles*, 40, e2025GB008822. <https://doi.org/10.1029/2025GB008822>
- Sass, J., Lachenbruch, A. H., & Munroe, R. J. (1971). Thermal conductivity of rocks from measurements on fragments and its application to heat-flow, determinations. *Journal of Geophysical Research*, 76(14), 3391–3401. <https://doi.org/10.1029/JB076i014p03391>
- Schaefer, K., Zhang, T., Slater, A. G., Lu, L., Etringer, A., & Baker, I. (2009). Improving simulated soil temperatures and soil freeze/thaw at high-latitude regions in the Simple Biosphere/Carnegie-Ames-Stanford Approach model. *Journal of Geophysical Research*, 114(F02021). <https://doi.org/10.1029/2008JF001125>
- Spencer, R. G., Aiken, G. R., Wickland, K. P., Striegl, R. G., & Hernes, P. J. (2008). Seasonal and spatial variability in dissolved organic matter quantity and composition from the Yukon River basin, Alaska. *Global Biogeochemical Cycles*, 22(4). <https://doi.org/10.1029/2008GB003231>
- Sturm, M., Holmgren, J., König, M., & Morris, K. (1997). The thermal conductivity of seasonal snow. *Journal of Glaciology*, 43(143), 26–41. <https://doi.org/10.3189/S002214300002781>
- Sturm, M. J., Holmgren, J., & Liston, G. E. (1995). A seasonal snow cover classification System for local to global applications. *Journal of Climate*, 8(5), 1261–1283. [https://doi.org/10.1175/1520-0442\(1995\)008<1261:ASSCCS>2.0.CO;2](https://doi.org/10.1175/1520-0442(1995)008<1261:ASSCCS>2.0.CO;2)
- Vonk, J. E., Tank, S. E., Mann, P. J., Spencer, R. G., Treat, C. C., Striegl, R., et al. (2015). Biodegradability of dissolved organic carbon in permafrost soils and aquatic systems: A meta-analysis. *Biogeosciences*, 12(23), 6915–6930. <https://doi.org/10.5194/bg-12-6915-2015>
- Vörösmarty, C. J., Federer, C. A., & Schloss, A. L. (1998). Potential evapotranspiration functions compared on US watersheds: Possible implications for global-scale water balance and terrestrial ecosystem modeling. *Journal of Hydrology*, 207(3–4), 147–169. [https://doi.org/10.1016/S0022-1694\(98\)00109-7](https://doi.org/10.1016/S0022-1694(98)00109-7)
- Willmott, C. J., Rowe, C. J., & Mintz, Y. (1985). Climatology of the terrestrial seasonal water cycle. *Journal of Climate*, 5(6), 589–606. <https://doi.org/10.1002/joc.3370050602>

- Yan, Z., Bond-Lamberty, B., Todd-Brown, K. E., Bailey, V. L., Li, S., Liu, C., & Liu, C. (2018). A moisture function of soil heterotrophic respiration that incorporates microscale processes. *Nature Communications*, 9(1), 1–10. <https://doi.org/10.1038/s41467-018-04971-6>
- Yi, Y., Kimball, J. S., Chen, R. H., Moghaddam, M., Reichle, R. H., Mishra, U., et al. (2018). Characterizing permafrost active layer dynamics and sensitivity to landscape spatial heterogeneity in Alaska. *The Cryosphere*, 12(1), 145–161. <https://doi.org/10.5194/tc-12-145-2018>
- Yi, Y., Kimball, J. S., Rawlins, M. A., Moghaddam, M., & Euskirchen, E. S. (2015). The role of snow cover affecting boreal-arctic soil freeze/thaw and carbon dynamics. *Biogeosciences*, 12(19), 5811–5829. <https://doi.org/10.5194/bg-12-5811-2015>
- Zeng, X., & Decker, M. (2009). Improving the numerical solution of soil moisture–based richards equation for land models with a deep or shallow water table. *Journal of Hydrometeorology*, 10(1), 308–319. <https://doi.org/10.1175/2008JHM1011.1>
- Zienkiewicz, O., & Taylor, R. (1991). *The finite element method, vol. 2 (solid and fluid mechanics, dynamics and nonlinearity)* (Vol. 620, pp. 227–229). McGraw-Hill.
- Zinke, P. J., Stangenberger, A. G., Post, W. M., Emanuel, W. R., & Olson, J. S. (1986). *Worldwide organic carbon and nitrogen data*. (Tech. Rep.). Oak Ridge, Tennessee.: Carbon Dioxide Information Center. (ORNL/CDIC-18).